

# 3D kinematics of white dwarfs from the SPY project \*

E.-M. Pauli<sup>1</sup>, R. Napiwotzki<sup>1</sup>, M. Altmann<sup>1</sup>, U. Heber<sup>1</sup>, M. Odenkirchen<sup>2</sup>, and F. Kerber<sup>3</sup>

<sup>1</sup> Dr. Remeis-Sternwarte, Astronom. Institut, Universität Erlangen-Nürnberg, Sternwartstr. 7, 96049 Bamberg, Germany

<sup>2</sup> Max-Planck-Institut für Astronomie, Königstuhl 17, 69117 Heidelberg, Germany

<sup>3</sup> Space Telescope European Coordinating Facility, ESO, Karl-Schwarzschild-Str. 2, 85748 Garching, Germany

## Abstract.

We present kinematics of a sample of 107 DA white dwarfs from the SPY project (ESO SN Ia Progenitor surveY) and discuss kinematic criteria for a distinction of thin disk, thick disk, and halo populations. This is the first homogeneous sample of white dwarfs for which 3D space motions have been determined.

Since the percentage of old stars among white dwarfs is higher than among main-sequence stars, they are presumably valuable tools in studies of old populations such as the halo and the thick disk. Studies of white dwarf kinematics can help to determine the fraction of the total mass of our Galaxy contained in the form of thick disk and halo white dwarfs, an issue which is still under discussion.

Radial velocities and spectroscopic distances obtained by the SPY project are combined with our measurements of proper motions to derive 3D space motions. Galactic orbits and further kinematic parameters are computed. We calculate individual errors of kinematic parameters by means of a Monte Carlo error propagation code. Our kinematic criteria for assigning population membership are deduced from a sample of F and G stars taken from the literature for which chemical criteria can be used to distinguish between thin disk, thick disk and halo. Candidates for thick disk and halo members are selected in a first step from the classical  $U-V$ -velocity diagram. Our final assignment of population membership is based on orbits and position in the  $J_z$ -eccentricity diagram. We find four halo and twelve thick disk white dwarfs.

We also present a systematic study of the effects of ignoring the radial velocity in kinematic investigations.

**Key words.** Stars: white dwarfs – Stars: kinematics – Galaxy: halo – Galaxy: thick disk – Galaxy: kinematics and dynamics

## 1. Introduction: population membership of white dwarfs

White dwarfs are the evolutionary end-products of most stars. As they are faint objects only the nearby objects have been detected so far. However, a large number of white dwarfs should be present in the Galaxy. Determining the contribution of white dwarfs to the total mass of the Galaxy could help solve one of the fundamental questions in modern astronomy: what is the nature of dark matter? The fact that the rotation curves of many galaxies are not Keplerian (Rubin et al. 1978) invokes the existence of additional dark matter distributed in a near-spherical structure, the so-called heavy-halo (Ostriker & Peebles 1973). It is estimated that for the Milky Way only 10% of the total mass are present in the form of stars, gas, and dust

in the Galactic disk and halo (Alcock et al. 2000). Dark matter candidates for the remaining 90% include exotic particles, cold molecular gas, and compact objects like black holes, white dwarfs and brown dwarfs. The role of white dwarfs in the dark matter problem is still uncertain. An open issue is the fraction of white dwarfs in the thick disk and halo populations and their fraction of the total mass of the Galaxy. In this context kinematic studies have proved a useful tool to decide on population membership of white dwarfs.

Sion et al. (1988) were the first to carry out kinematic investigations of a large sample of white dwarfs from the first edition of the McCook & Sion catalogue (McCook & Sion 1987). They found a fraction of about 10% halo white dwarfs.

Another method for a distinction of the disk and halo populations was proposed by Garcia-Berro et al. (1999): they developed a neural network to classify a subsample of the McCook & Sion stars (McCook & Sion 1987) in a five dimensional parameter space by means of synthetic halo

Send offprint requests to: E.-M. Pauli (pauli@sternwarte.uni-erlangen.de)

\* Based on observations obtained at the Paranal Observatory of the European Southern Observatory for programs 165.H-0588 and 167.D-0407

and disk tracer stars generated with a Monte Carlo simulation. Their results confirm those of Sion et al. (1988).

Liebert et al. (1989) investigated a sample of 43 spectroscopically confirmed white dwarfs from the LHS catalogue (Luyten 1979). They obtained a percentage of 14% halo white dwarfs. They were also the first to derive a luminosity function of halo white dwarfs.

Recently Oppenheimer et al. (2001) have completed a deep proper motion survey towards the South Galactic Cap, and claim detection of 38 halo white dwarfs. Most of the white dwarfs have featureless DC spectra and therefore radial velocities could not be measured. The Galactic radial ( $U$ ) and rotational ( $V$ ) velocity components were calculated from photometric distances and proper motions alone. The velocity component  $W$  perpendicular to the Galactic disk was set to zero arguing that in the direction of the South Galactic Cap the tangential motion is not a function of  $W$ . Their results are presented in the form of a  $U$ - $V$ -velocity diagram with superposed  $1\sigma$  and  $2\sigma$  contours for the expected locations of the thick disk and halo components of the Galaxy. White dwarfs lying outside the  $2\sigma$  contours of the disk are assumed to belong to the heavy halo.

However, this result is discussed controversially: e.g. Reid et al. (2001) claimed that the velocity distribution of the so-called heavy halo white dwarfs is more consistent with the high velocity tail of the thick disk. The major difference between the two investigations is that Oppenheimer et al. (2001) adopted  $W = 0 \text{ km s}^{-1}$  whereas Reid et al. (2001) set  $v_{\text{rad}} = 0 \text{ km s}^{-1}$ .

The common problem of the investigations discussed above is the lack of radial velocity measurements. Especially deviating conclusions derived from the white dwarfs of the Oppenheimer et al. (2001) sample demonstrate that different assumptions on the values of  $v_{\text{rad}}$  can produce different fractions of halo and thick disk stars and thus have effects on the determination of the white dwarf halo density. Therefore a sample of white dwarfs with known radial velocity measurements is needed in order to obtain the full 3D kinematic information and to study the effects of setting  $v_{\text{rad}}$  to zero. Once this effect is well understood samples of stars can be dealt with for which no radial velocity information is available, e.g. in the case of cool white dwarfs.

Silvestri et al. (2001) presented kinematics of 41 white dwarfs in common proper motion binary systems. Radial velocities could be easily measured from the sharp lines in the spectrum of the cool companion star. Thus they could calculate all three velocity components  $U$ ,  $V$ , and  $W$ . The mean values and standard deviations of those indicate that most of the sample stars belong to the thick disk. Three white dwarfs (7%) were found to be belonging to the halo.

In a more recent study, Silvestri et al. (2002) investigated kinematics of another 116 white dwarfs with M dwarf companions. They detected 13 high velocity white dwarfs and concluded that 12 of them belong to the thick disk as their M dwarf companions have near solar abundance levels. They compared the effect of assuming either

$v_{\text{rad}}$  or  $W$  to be zero and discovered that the effect of  $v_{\text{rad}} = 0 \text{ km s}^{-1}$  is negligible, whereas  $W = 0$  changes the fraction of high velocity white dwarfs.

We present a sample of DA white dwarfs from the ESO **SN Ia Progenitor surveY** (SPY) by Napiwotzki et al. (2001) which is ideal for probing population membership of white dwarfs. The SPY sample allows us to overcome several limitations of previous investigations. When investigating DA white dwarfs, radial velocities can be measured from the shifts of the Balmer lines which is an advantage over DC white dwarfs where no spectral lines are present. Due to high resolution UVES VLT spectra we can benefit from radial velocities of unprecedented precision (errors of only  $2 \text{ km s}^{-1}$ ) and spectroscopic distances (relative errors of only 10%) from Napiwotzki et al. (2003, in prep.). We supplemented these data with proper motion measurements of fair quality (typical errors about  $20 \text{ mas yr}^{-1}$ ). Therefore we possess a very homogeneous set of radial and tangential velocity information with individual errors for each star. Contrary to previous studies we do not only consider the classical velocity components  $U$ ,  $V$ , and  $W$  of each white dwarf but calculate its orbit in the Galactic disk. This allows us to define new sophisticated criteria for classifying thin, thick disk, and halo populations by considering orbits and kinematic parameters. Another important question is how errors of the input parameters affect errors of the kinematic output parameters. An error propagation code using a Monte Carlo simulation has been developed which allows us to check the statistical significance of our results. We use our sample to test the results of the samples which lack radial velocity information by investigating the effect of setting our radial velocities arbitrarily to zero.

Our publication is structured as follows: Sect. 2 deals with the data and the error analysis. In Sect. 3 our analysis method is described and the calibration sample is presented. Sect. 4 is dedicated to our kinematic studies, focusing on classical and more sophisticated analysis methods. Our results appear in Sect. 5 and are discussed in Sect. 6. We finish with conclusions in Sect. 7.

## 2. Input data and error treatment

### 2.1. Input data

Our sample consists of 107 DA white dwarfs from the SPY project analysed by Koester et al. (2001). Input stars for the SPY project were drawn from the catalogue of McCook & Sion (1999), the Montreal-Cambridge-Tololo (MCT) survey (Lamontagne et al. 2000), the Edinburgh-Cape (EC) survey (Kilkenny et al. 1997), the Hamburg/ESO Survey (Wisotzki et al. 1996, 2000; Christlieb et al. 2001), and the Hamburg Quasar Survey (Hagen et al. 1995; Homeier et al. 1998). The selection criteria were spectroscopic confirmation as white dwarf (at least from objective prism spectra) and  $B < 16.5$  or  $V < 16.5$ , respectively. As the stars are compiled from a number of different sources we cannot expect com-

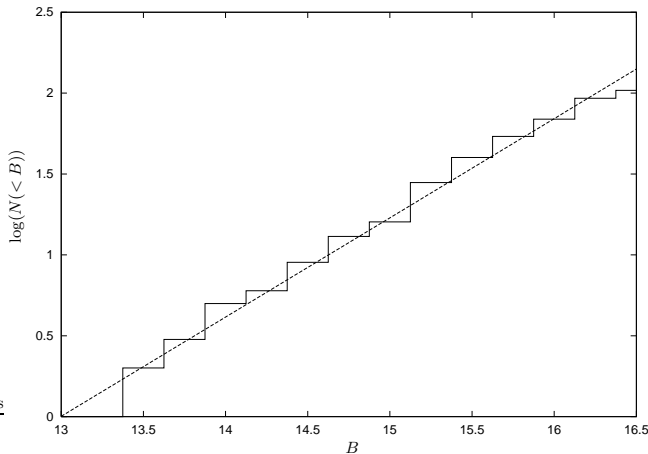


**Fig. 1.** Cumulative Number density as a function of  $B$ -magnitude

completeness. To make more quantitative statements on the level of incompleteness we compared our sample with the subsample of DA white dwarfs from the Palomar-Green Ultraviolet-Excess Catalog (Green et al. 1986). In Fig. 1 the cumulative number density is plotted as a function of  $B$ -magnitude. A linear function is fitted to the curve to obtain the count slope  $\frac{d(\log N)}{dB} = 0.61 \pm 0.02$ . This value does not differ much from 0.57 derived by Green et al. (1986). They estimated the completeness level for DA white dwarfs to be 77%. Thus, though it is difficult to compare the two samples this comparison demonstrates that at least no magnitude dependent bias is produced in the SPY sample.

Radial velocities and spectroscopic distances were taken from Napiwotzki et al. (2003, in prep.). The aim of the SPY project is to detect radial velocity (RV) variable close binary white dwarfs. Two spectra at different epochs are taken and checked for RV variations. Since orbital motions distort the measurement of space motions, RV variable stars were discarded from our sample.

Proper motion components  $\mu_\alpha \cos \delta$  and  $\mu_\delta$  were obtained from photographic plate data from the ESO Online Digitized Sky Survey (DSS1, DSS2)<sup>1</sup> and the USNO catalogue (Monet et al. 1998). The Digitized Sky Survey (DSS) is a collection of (red) photographic Schmidt plate that have been digitised. One pixel corresponds to  $1.7''$  on the DSS1 and to  $1''$  on the DSS2 plates. In order to demonstrate that DSS data are suitable for astrometry we compared coordinates obtained on DSS1 plates with two different software packages, SExtractor (Bertin & Arnouts 1996) and DAOPHOT (Stetson 1992). The sigma of the differences in the coordinates was 0.02 pixel, i.e.  $0.035''$ . This indicates that our results are robust, i.e. they do not depend much on the star extraction software used.

Each star identified on the images was assigned a number and  $x, y$ - coordinates were determined for the centroid of the star using SExtractor software (Bertin & Arnouts

1996). From the USNO archive a catalogue of stars (with  $\alpha$  and  $\delta$ ) within a region of  $10'$  around the coordinates of the white dwarf was extracted. The next step was to identify some stars on the DSS1/DSS2 image with the corresponding USNO stars. After that an astrometric solution for the plates was created and proper motions were calculated with a software package developed by Geffert et al. (1997). We did not measure absolute but only relative proper motions. To obtain absolute proper motions it would be necessary to use background galaxies on the plates as a reference. But it is difficult to identify faint galaxies on DSS images. So we lack the link to the extragalactic system. We take this into account by adopting a systematic error of  $5 \text{ mas yr}^{-1}$ . For details we refer to Altmann (2002).

To the systematic error we add an error depending on the epoch difference  $\Delta t$  (in years) of the DSS1 and DSS2 plates of  $200 \text{ mas yr}^{-1} / \Delta t$ . We assumed an accuracy of 0.1 pixel for measuring positions on the DSS plates (this assumption is more conservative than the 0.02 pixel mentioned above). This accuracy corresponds to 170 mas and 100 mas on the DSS1 and DSS2 plates, respectively. The total error is, by linear error propagation,  $\sqrt{170^2 + 100^2} = 200$  mas. We divide it by the epoch difference  $\Delta t$  to obtain the error in  $\mu_\alpha \cos \delta$  and  $\mu_\delta$ .

For our sample this results in an error of about  $18 \text{ mas yr}^{-1}$  for a typical epoch difference of 15 yr. Since most DSS1 plates of the Southern hemisphere were taken in the seventies, the typical epoch difference does not exceed 15 years which is the limiting factor for the accuracy of the proper motion measurements. Nevertheless as our sample stars are near ( $d \leq 500 \text{ pc}$ ), the proper motion errors do not lead to high errors in the tangential velocities.

Additional proper motions were extracted from the UCAC catalogue (Zacharias et al. 2000) for stars for which no DSS2 data are available. The UCAC programme is an ongoing, astrometric, observational program, which started in February 1998. A global sky coverage is expected by end of 2003. For those stars of our sample where both UCAC and our own measurements of proper motions were available we compared the values of  $\mu_\alpha \cos \delta$  and  $\mu_\delta$  and found them to be in accordance (within the error ranges). This demonstrates that our error margins have been chosen sensibly and provides a successful test for the reliability of our astrometric measurements.

The input parameters radial velocities, spectroscopic distances (Napiwotzki et al. 2003, in prep.) and proper motion components together with their errors are listed for all white dwarfs in Table 1. In column 2 of this table the number of spectra available for each white dwarf is indicated. If only one spectrum is available we cannot rule out a possible binarity of the objects. Nevertheless, we keep them in our sample because only about 15% of the white dwarfs investigated by the SPY project (Napiwotzki et al. 2001) are radial velocity variable. From this we might expect about four stars in Table 1 to be radial velocity (RV) variable.

<sup>1</sup> the DSS1/DSS2 data can be downloaded from e.g. <http://archive.eso.org/dss/dss>

## 2.2. The Monte Carlo error propagation code

An error propagation code based on a Monte Carlo method (Gershenfeld 1999) was developed in order to take errors into account. Let  $x_0$  be an input parameter of a numerical code and  $\sigma$  its corresponding error. The error of the output parameter  $z$  is obtained as follows: first a large number of representative (e.g. 1 000)  $x$ -values obeying a Gaussian distribution (with  $x_0$  as mean value and  $\sigma$  as standard deviation) is chosen. Then  $z$  is computed for each  $x$  and the mean value and the error of  $z$  are calculated. Instead of using only one input parameter it is possible to deal with several input parameters which are varied simultaneously. This method can be useful in cases where a direct error propagation cannot be carried out due to the complexity of the problem.

We applied our error propagation code to the Odenkirchen & Brosche (1992) code described in Sect. 3.1 for calculating errors of the kinematic parameters of the white dwarfs in our sample. Input parameters were radial velocities, proper motion components and spectroscopic distances together with their corresponding errors. Then 1 000 representative values of  $v_{\text{rad}}$ ,  $\mu_\alpha \cos\delta$ ,  $\mu_\delta$  and  $d$  obeying a Gaussian distribution were chosen simultaneously and the output parameters together with their errors were computed.

## 3. Our kinematic analysis method

Coordinates  $\alpha$  and  $\delta$ , proper motion components, distances and radial velocities allow us to benefit from the full 3D information on Galactic positions and velocities of the white dwarfs. These quantities can be transformed to the Galactic system to obtain the coordinates  $X, Y$ , and  $Z$  and the velocity components  $U$  (in the Galactic disk in direction towards the Galactic centre),  $V$  (in the direction of the Galactic rotation) and  $W$  (perpendicular to the Galactic disk). We adopt the IAU standard (Kerr & Lynden-Bell 1986) of  $R_0 = 8.5$  kpc for the distance of the sun from the Galactic centre and  $V(R_0) = 220 \text{ km s}^{-1}$  for the rotational velocity at the sun's position. For the solar peculiar motion we take the values of Dehnen & Binney (1998):  $U_{\text{solar}} = 10 \text{ km s}^{-1}$ ,  $V_{\text{solar}} = 5.25 \text{ km s}^{-1}$  and  $W_{\text{solar}} = 7.17 \text{ km s}^{-1}$ .

Having calculated  $U$ ,  $V$ , and  $W$  the classical analysis in the  $U$ - $V$ -velocity diagram yields information on population membership. This is possible because we have a local sample. Furthermore we make use of more sophisticated analysis tools (see Sect. 4.2 and Sect. 4.3). Given a Galactic potential the observed values of  $X$ ,  $Y$ ,  $Z$  and  $U$ ,  $V$ ,  $W$  can be used to integrate the equation of motion of the star and to follow the dynamical evolution of these quantities over time. The result is the orbit of the star in the Galaxy. At this point it should be noted that this orbit cannot be taken as real but is an idealised representation. Taken the initial conditions of a white dwarf at the present time it cannot necessarily be extrapolated where it will be after a certain time has elapsed, because the mean-field approximation for the Galactic potential

is simplified and scattering processes between individual stars are neglected. But the advantage of this approach is that orbital parameters (such as the eccentricity or the angular momentum) can be computed which allow us to gain additional information on the population-membership of the white dwarfs.

## 3.1. Calculation of orbits and kinematic parameters

For the computation of orbits and kinematic parameters we used a code by Odenkirchen & Brosche (1992) based on a Galactic potential by Allen & Santillan (1991). This potential is completely analytical, symmetrical with respect to the  $Z$ -axis, time-independent and fitted to the observational values of the Galactic rotation curve and the perpendicular force. For the integration of the equations of motion Odenkirchen & Brosche (1992) implemented the Bulirsch-Stoer extrapolation method with adaptive step-size. Input parameters are  $\alpha(2000)$ ,  $\delta(2000)$ ,  $d$ ,  $v_{\text{rad}}$ ,  $\mu_\alpha \cos\delta$ ,  $\mu_\delta$ . The motion of the star was followed for a time span of 2 Gyr with a time-step of 0.001 Gyr.

$X$ ,  $Y$ ,  $Z$  and  $U$ ,  $V$ ,  $W$  were calculated as a function of time. Output parameters are the total energy  $E$  and  $z$ -component of angular momentum  $J_Z$ , orbital quantities like the perigalactic distance  $R_{\text{min}}$ , the apogalactic distance  $R_{\text{max}}$ , the eccentricity  $e = \frac{R_{\text{max}} - R_{\text{min}}}{R_{\text{max}} + R_{\text{min}}}$  and the maximal height above the Galactic disk  $z_{\text{max}}$ .

In order to check if our results depend on the choice of a special Galactic potential we recalculated orbits and kinematic parameters with another potential taken from Flynn et al. (1996) and compared them to those obtained with the potential of Allen & Santillan (1991). We found that the changes are small and do not affect our classification criteria for distinction of the different populations. While  $J_Z$  is not altered at all, the eccentricity typically reduces by only 0.01 and the character of the orbits (thin disk, thick disk or halo type) stays the same though the orbits are changed slightly. This provides a justification that our results do not depend sensitively on the choice of a particular potential.

## 3.2. The calibration sample

Unlike for main-sequence stars the population membership of white dwarfs cannot be determined from spectroscopically measured metallicities. Therefore we have to rely on kinematic criteria. Those criteria have to be calibrated using a suitable calibration sample of main-sequence stars. In our case this sample consists of F and G main-sequence stars from Edvardsson et al. (1993), Fuhrmann (1998), and Fuhrmann (2000, <http://www.xray.mpe.mpg.de/fuhrmann/>).

For both samples a detailed abundance analysis has been carried out. Fuhrmann found that the disk and halo populations can be distinguished best in the  $[\text{Mg}/\text{Fe}]$  versus  $[\text{Fe}/\text{H}]$  diagram. Halo and thick disk stars can be separated by means of their  $[\text{Fe}/\text{H}]$  abundances. Halo and

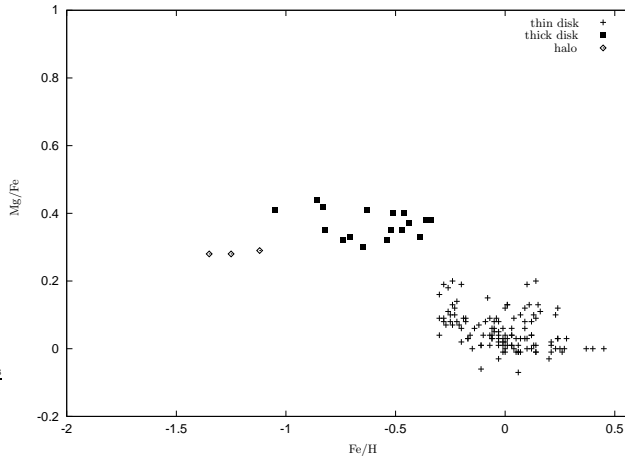


**Fig. 2.** [Mg/Fe]-[Fe/H] abundance-diagram for the main-sequence stars of the calibration sample

thick disk stars possess a higher [Mg/Fe] ratio than thin disk stars ( $\alpha$  Process enhanced).

We selected a subsample of 137 from the Fuhrmann and Edvardsson stars for which distances and proper motion are available at the ARI Database for Nearby Stars (<http://www.ari.uni-heidelberg.de/aricns>). Radial velocities were obtained from the ARI Database as well or the compilation of Barbier-Brossat et al. (1994). Those parameters are necessary to compare the kinematics of the main-sequence stars with those of the white dwarfs. In Fig. 2 the [Mg/Fe] versus [Fe/H] abundances for the 137 main-sequence stars are shown. Those stars are divided into halo, thick disk and thin disk according to their position in the diagram following Fuhrmann (2000). The halo stars have  $[\text{Fe}/\text{H}] < -1.2$ , the thick disk stars  $-1.1 \leq [\text{Fe}/\text{H}] \leq -0.3$  and  $[\text{Mg}/\text{Fe}] \geq 0.3$  and the thin disk stars  $[\text{Fe}/\text{H}] > -0.3$  and  $[\text{Mg}/\text{Fe}] \leq 0.2$ . Stars in the overlapping area between the thin and the thick disk were neglected in order to ensure a clear distinction between the two disk populations. Due to the low number of halo and thick disk stars in the calibration sample the separation between these two populations is somewhat arbitrary, but as will be demonstrated later, halo and thick disk stars show very distinct kinematic properties so that they cannot be confused easily.

The star HD 148816 is classified as thick disk star by means of its abundances ( $[\text{Fe}/\text{H}] = -0.74$ ,  $[\text{Mg}/\text{Fe}] = 0.32$ ). However it will be demonstrated later in Sect. 4.1 and Sect. 4.2 that its kinematics are not compatible with a thick disk but a halo member. Therefore we will exclude this star from the calibration sample.

#### 4. Kinematic studies

We calculated orbits and kinematic parameters for all white dwarfs (see Table 2) and all main-sequence stars for intercomparison. For our white dwarf sample the errors of  $e$ ,  $J_Z$ ,  $U$ ,  $V$ ,  $W$  were computed with our Monte

Carlo error propagation code described in Sect. 2.2. They can be found in Table 2 as well.

#### 4.1. The $U$ - $V$ -velocity diagram

A classical tool for kinematic investigations is the  $U$ - $V$ -velocity diagram. In Fig. 3  $U$  is plotted versus  $V$  for the main-sequence stars. Thin disk stars are marked by crosses, thick disk stars by squares, and halo stars by diamonds. For all disk stars the mean values and standard deviations of the two velocity components have been calculated:  $\langle U_{\text{ms}} \rangle = -0.3 \text{ km s}^{-1}$ ,  $\langle V_{\text{ms}} \rangle = 195 \text{ km s}^{-1}$ ,  $\sigma_{U_{\text{ms}}} = 41 \text{ km s}^{-1}$ ,  $\sigma_{V_{\text{ms}}} = 39 \text{ km s}^{-1}$ . The  $1\sigma$  and  $2\sigma$ -contours are shown in Fig. 3. Chiba & Beers (2000) found  $\sigma_V = 50 \text{ km s}^{-1}$ ,  $\sigma_U = 46 \text{ km s}^{-1}$  for the thick disk. Most of the thin disk stars stay within the  $2\sigma$ -contours. The area outside the  $2\sigma$ -limit contains all halo and many of the thick disk stars. The three halo main-sequence stars are characterised by values of  $\sqrt{U^2 + (V - 195)^2} \geq 150 \text{ km s}^{-1}$ . As already mentioned we ignore the thick disk star HD 148816 for kinematic studies. It stands out by its peculiar position in the  $U$ - $V$ -diagram with a negative value of  $V$ .

In Fig. 4 the  $U$ - $V$ -plot is shown for the white dwarfs with error bars. For comparison the  $1\sigma$  and  $2\sigma$ -contours derived for the main-sequence stars appear as well. In order to detect halo and thick disk stars we concentrate on the 14 white dwarfs outside the  $2\sigma$ -limit. Four stars have  $\sqrt{U^2 + (V - 195)^2} \geq 150 \text{ km s}^{-1}$ . WD 0252-350 and WD 2351-368 have a  $V$  velocity around  $30 \text{ km s}^{-1}$  which is clearly below the  $220 \text{ km s}^{-1}$  of the local standard of rest and their  $U$  values are high. This indicates that they do not rotate with the Galactic disk and can move far away from the Galactic centre. This is characteristic for halo stars. WD 1448+077 and WD 1524-749 do even have a negative value of the  $V$ -velocity, which means that their orbits are retrograde. They therefore do not belong to the disk. We also found a main-sequence star (HD 194598) on a retrograde orbit which according to its abundance pattern is a member of the halo. The other 10 white dwarfs outside the  $2\sigma$ -contours are possible thick disk candidates belonging to the high velocity tail (large deviations in  $U$  and  $V$  from the disk mean values) of the disk.

#### 4.2. The $J_Z$ -eccentricity-diagram

The  $U$ - $V$ -plot is not the only source of information about population membership. Two important orbital parameters are the  $z$ -component of the angular momentum  $J_Z$  and the eccentricity of the orbit  $e$ . Both are plotted against each other for the main-sequence stars in Fig. 5. The different populations can be distinguished well in this diagram. The thin disk stars cluster in an area of low eccentricity and  $J_Z$  around  $1800 \text{ kpc km s}^{-1}$ , which we denote by Region 1.

The thick disk stars possess higher eccentricities and lower angular momenta. They can be found in Region 2.

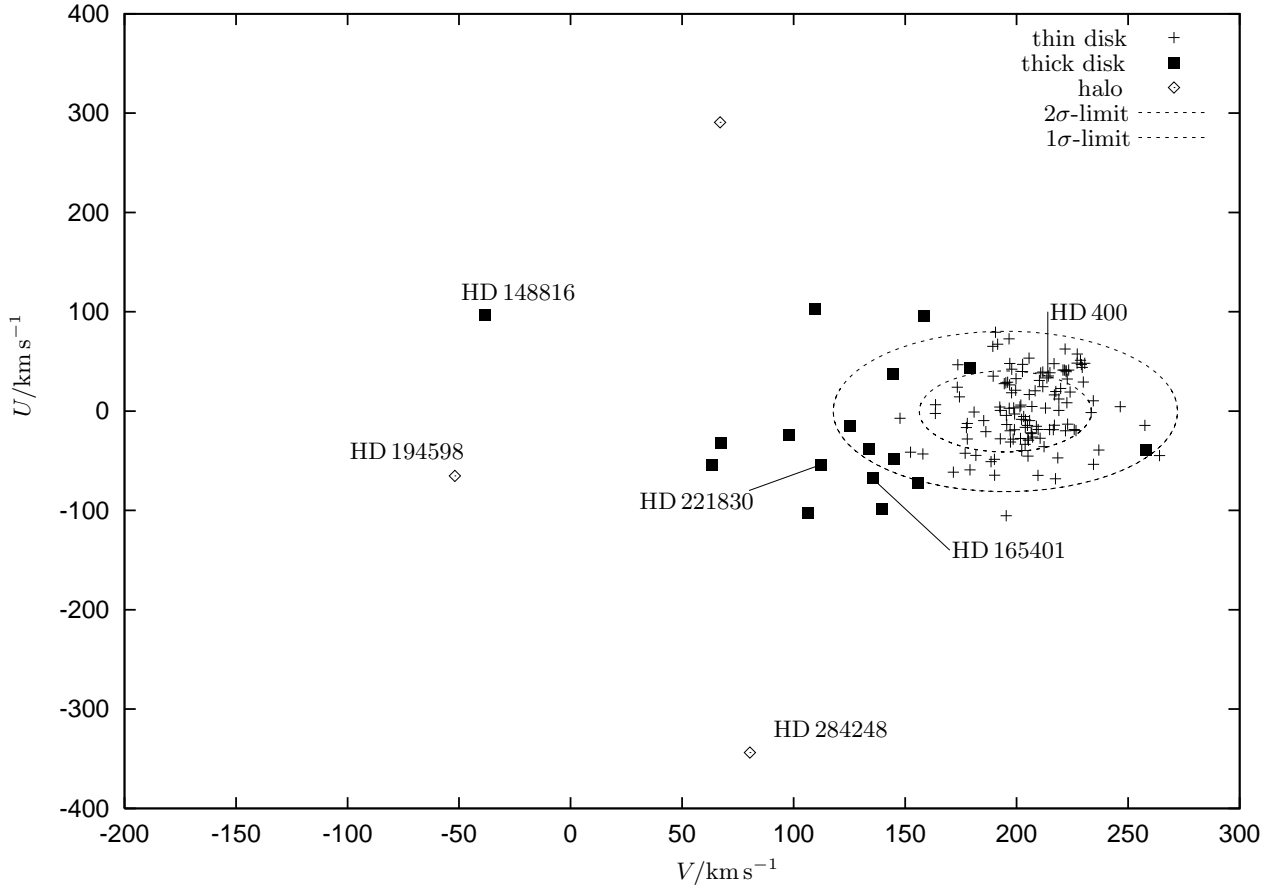


**Fig. 3.**  $U$ - $V$ -velocity diagram for the main-sequence stars, dashed lines:  $1\sigma$ -,  $2\sigma$ -contours, symbols with numbers are stars mentioned in the text

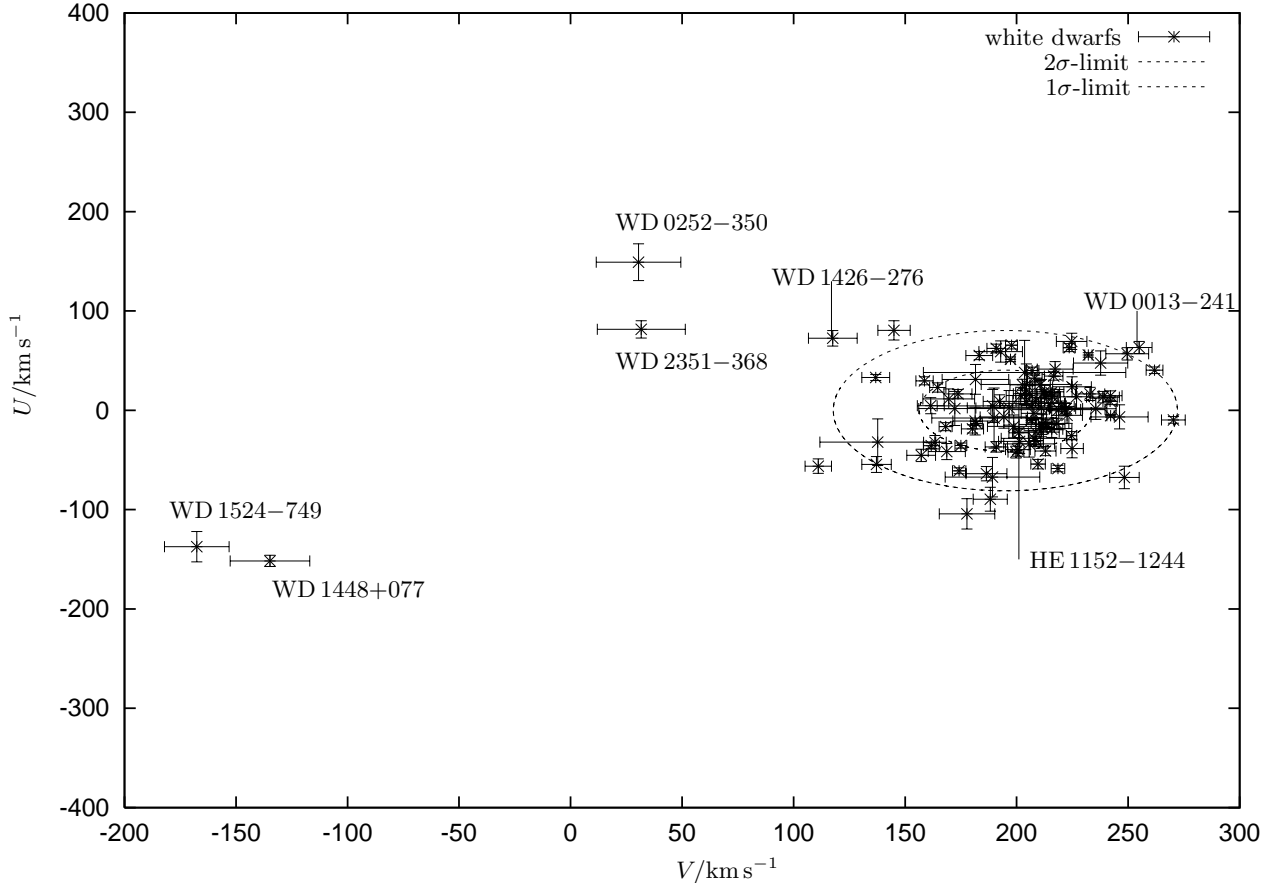


**Fig. 4.**  $U$ - $V$ -velocity diagram for the white dwarfs with  $1\sigma$ -,  $2\sigma$ -contours from Fig. 3, symbols with numbers are white dwarfs mentioned in the text

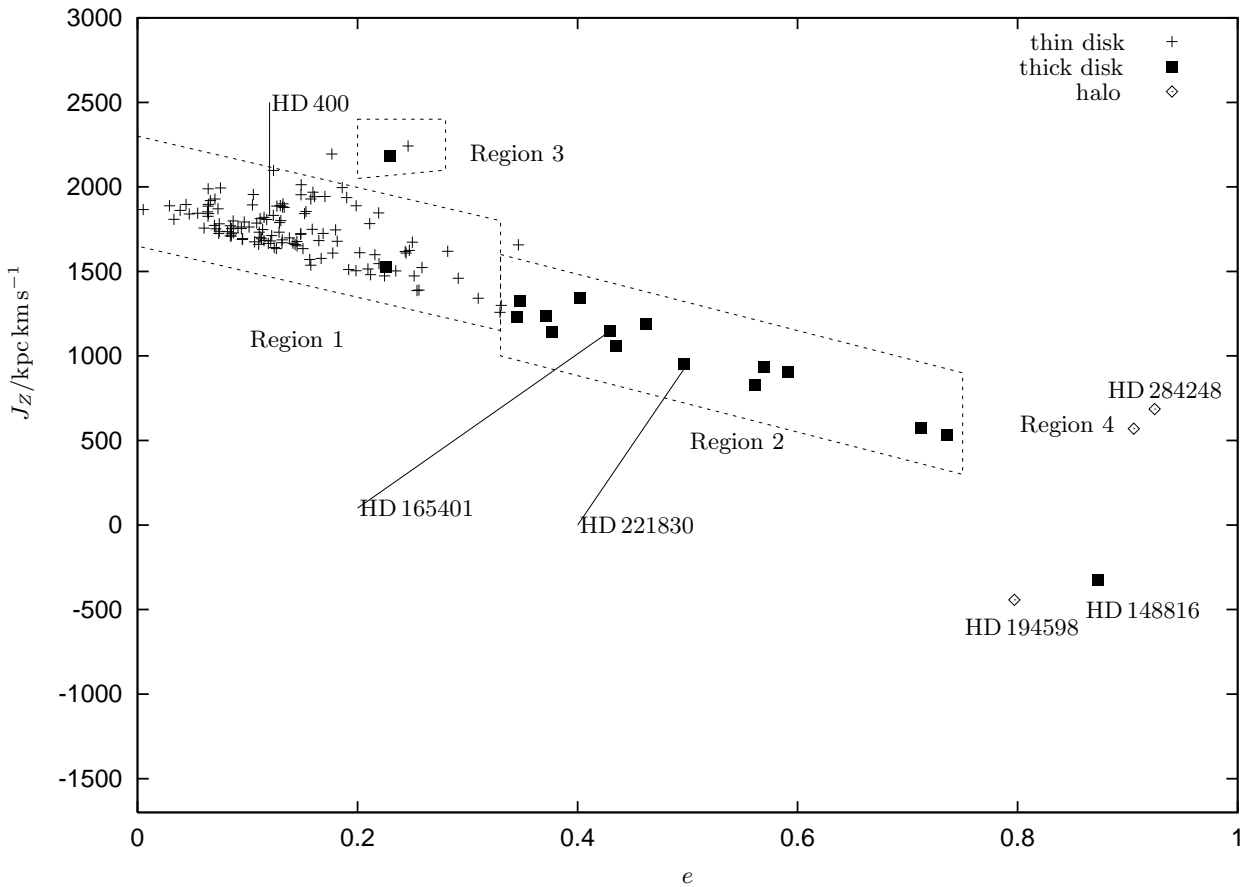


**Fig. 5.**  $J_z$ - $e$ -diagram for the main-sequence stars, symbols with numbers are stars mentioned in the text

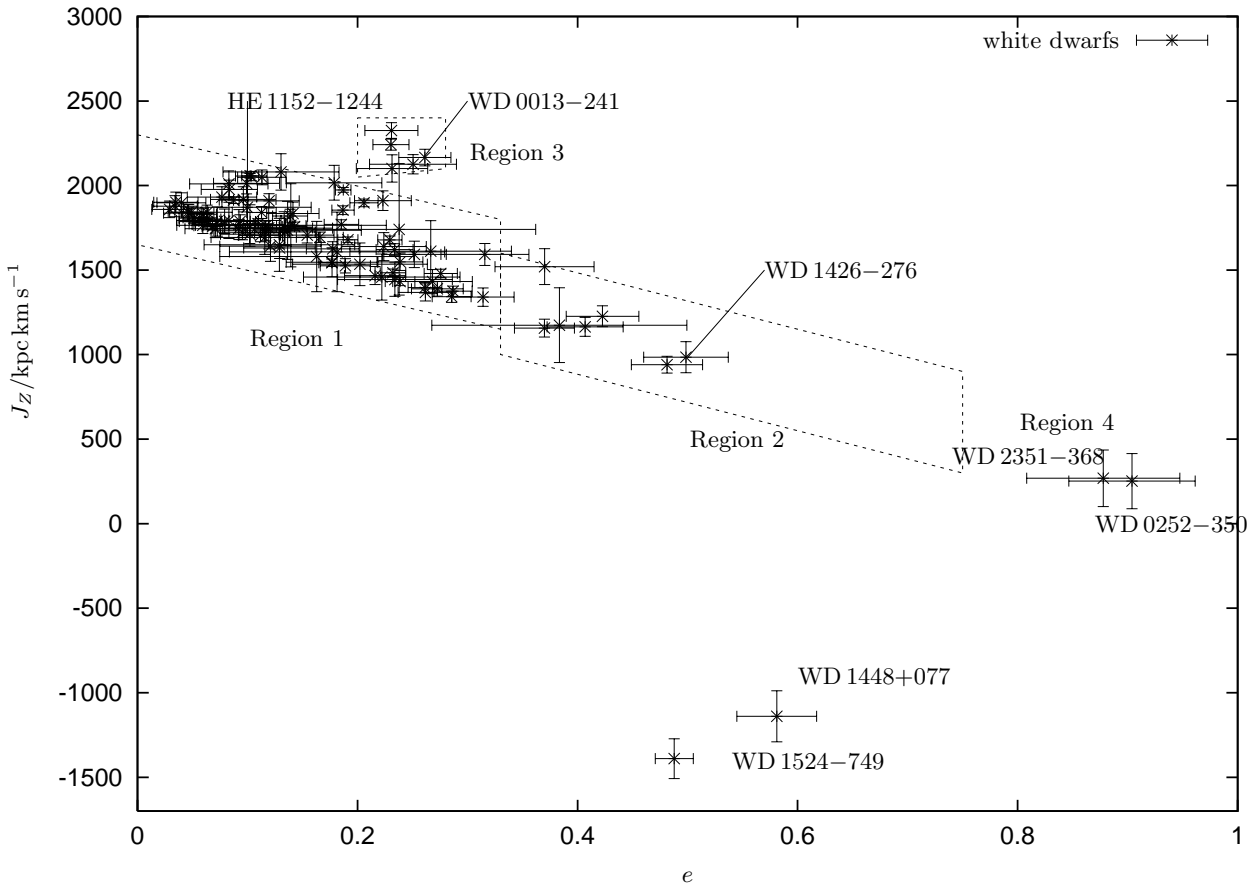


**Fig. 6.**  $J_z$ - $e$ -diagram of the white dwarfs, symbols with numbers are white dwarfs mentioned in the text

Two stars, one from the thin disk and one from the thick disk, populate an intermediate Region 3 with eccentricity around  $e = 0.22$  and large  $J_Z$ . The reason for defining this additional Region 3 is that (as will be seen in Fig. 6) five white dwarfs that do neither belong to Region 1 nor to Region 2 can be found there. The halo stars with very high eccentricity and smaller  $J_Z$  can be found in Region 4. This region also contains the star HD 148816 which suggests again that this star really belongs to the halo and not to the thick disk.

In Fig. 6 the  $J_Z$ - $e$ -diagram for the white dwarfs is shown with the different regions as defined above. Let us first concentrate on the four halo white dwarf candidates. WD 0252–350 and WD 2351–368 are the stars with the largest eccentricity, they lie very close to the halo main-sequence stars. WD 1448+077 and WD 1524–749 again populate an exceptional region in the diagram. Their value of  $J_Z$  is negative. Their eccentricity is not as large as that of the other halo stars.

Five of the ten thick disk candidates lying outside the  $2\sigma$ -limit in the  $U$ - $V$ -velocity diagram are present in Region 2. Two stars, WD 1952–206 and WD 0204–233 did not appear outside the  $2\sigma$ -limit, but they are clearly situated in Region 2.

Five white dwarfs can be found in Region 3. Four of them have already been classified as possible thick disk members in the  $U$ - $V$ -plot, only WD 0509–007 is a new thick disk candidate.

Of the 10 thick disk candidates in the  $U$ - $V$ -plot, 9 are present in Regions 2 and 3. Three additional thick disk candidates only show up in the  $J_Z$ - $e$ -diagram. Hence the  $U$ - $V$ -velocity plot alone is not sufficient to decide on population membership. The  $J_Z$ - $e$ -diagram can provide further information.

#### 4.3. Orbits

The eccentricity was extracted from the orbit of the white dwarfs. It can also be interesting to look at the orbits themselves. We consider the motion perpendicular to the plane (in the  $Z$ -direction) as a function of the motion inside the plane in radial direction ( $\rho = \sqrt{X^2 + Y^2}$ ). This is called the meridional plot. We compare meridional plots of main-sequence and white dwarf stars of the different populations. For ease of comparison the scale is the same for all plots.

We start with the thin disk stars. Fig. 7 shows the orbit of HD 400, a typical main-sequence thin disk star. It is situated in Region 1 in the  $J_Z$ - $e$ -diagram and its extensions in the  $\rho$  and the  $Z$ -directions are small. The white dwarf HE 1152–1244 (Fig. 8) has an orbit similar to that of HD 400 suggesting that it belongs to the thin disk. Actually most of our white dwarfs possess thin disk meridional plots similar to this one.

The orbit of the main-sequence star HD 284248 (Fig. 9) is characteristic for a halo object. Its extension in  $\rho$  is so large that it exceeds the range of the plot (18 kpc) and

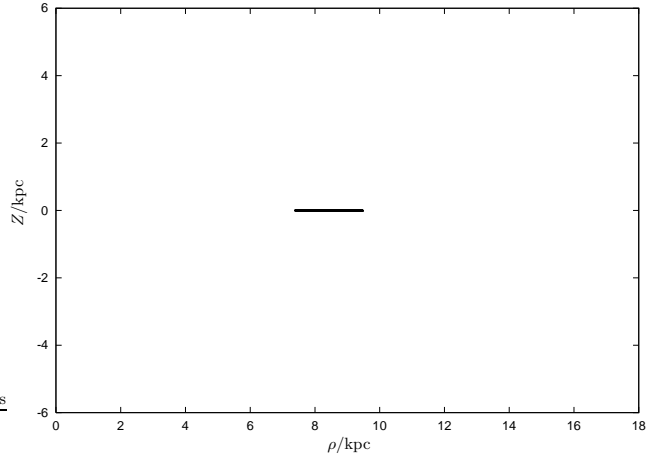


Fig. 7. Orbit of HD 400, a thin disk main-sequence star

its vertical distance from the Galactic plane is larger than 6 kpc. Due to their orbits the white dwarfs WD 0252–350 (Fig. 10) and WD 2351–368 also qualify as halo stars. The white dwarfs WD 1448+0077 and WD 1524–749 with negative  $V$  velocity (retrograde orbit) are compared with the main-sequence halo star (HD 194598) which has a similar  $V$ -velocity. The meridional plot of HD 194598 (Fig. 11) has smaller vertical and meridional distances but a large eccentricity. We know from its abundance pattern and the  $U$ - $V$ -plot and  $J_Z$ - $e$  plot that it must belong to the halo. WD 1448+0077's (Fig. 12) and WD 1524–749's orbits are nearly identical to that of HD 194598. Hence we conclude that they are members of the halo population, too.

The thick disk main-sequence stars are characterised by orbits more extended in the  $\rho$  and  $Z$  directions than that of a thin disk star. However, they do not cover such a large region in the meridional plot as a halo member. Examples are the orbits of the thick disk members HD 221830 (Fig. 13) and HD 165401 (Fig. 15).

The next step is to compare those orbits to the orbits of our white dwarf thick disk candidates. Those are all 13 white dwarfs lying either outside the  $2\sigma$ -limit in the  $U$ - $V$ -diagram or in Regions 2 or 3 in the  $J_Z$ - $e$ -diagram. Four of the thick disk candidates possess meridional plots similar to that of HD 221830. As an example the orbit of WD 1426–276 is shown in Fig. 14. Nine of our candidates possess orbits like HD 165401. A representative is the white dwarf WD 0013–241 (Fig. 16).

## 5. Results

For a refined classification of population membership of our white dwarf sample we combine all three criteria discussed above.

Characteristic for halo white dwarfs is a value of  $\sqrt{U^2 + (V - 195)^2} \geq 150 \text{ km s}^{-1}$  and their location in Region 4 in the  $J_Z$ - $e$ -diagram. Their orbits typically have high extensions in  $\rho$  and  $Z$  like HD 284248. WD 0252–350 and WD 2351–368 fulfil these criteria and are therefore classified as halo white dwarfs. Stars with retrograde or-

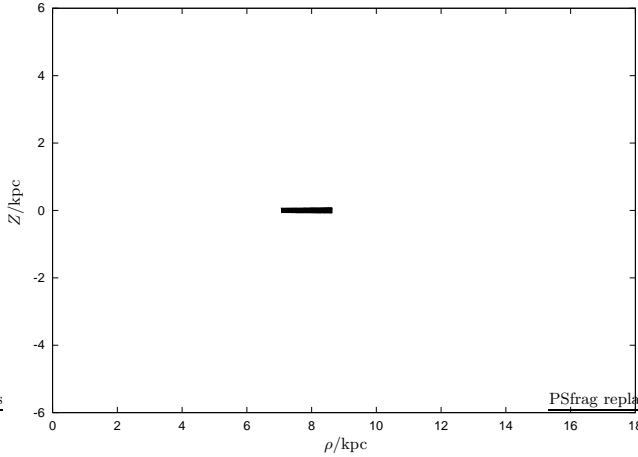


**Fig. 8.** Orbit of HE 1152–1244, a thin disk white dwarf

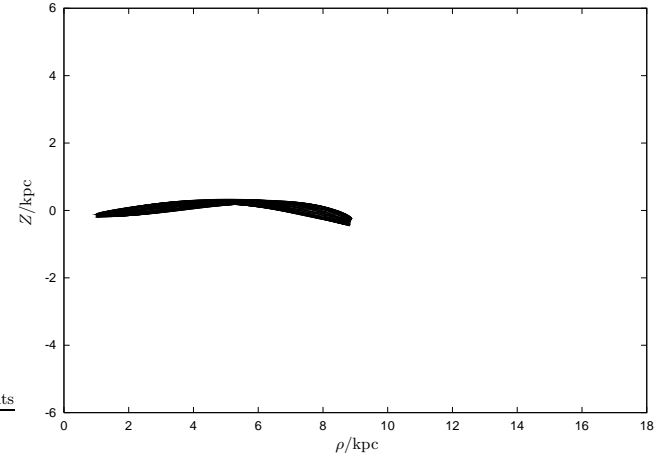


**Fig. 11.** Orbit of HD 194598, a retrograde halo main-sequence star

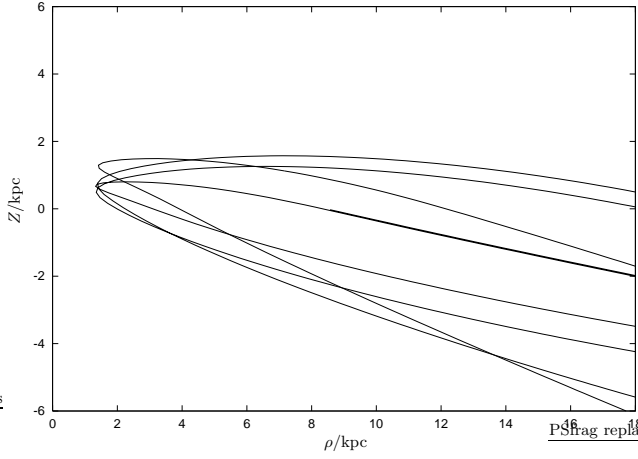


**Fig. 9.** Orbit of HD 284248, a halo main-sequence star

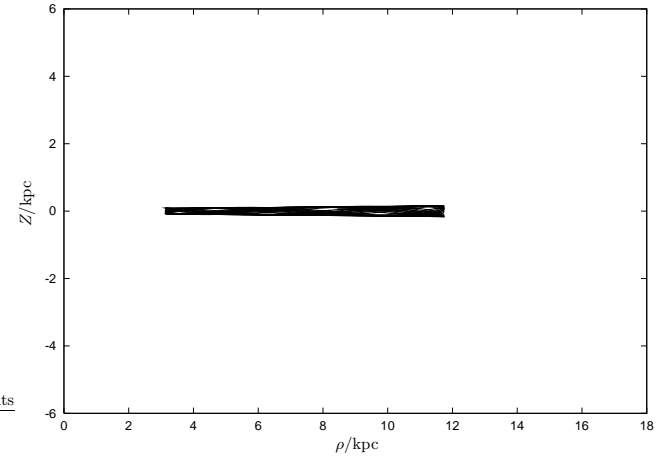


**Fig. 12.** Orbit of WD 1448+077, a retrograde halo white dwarf

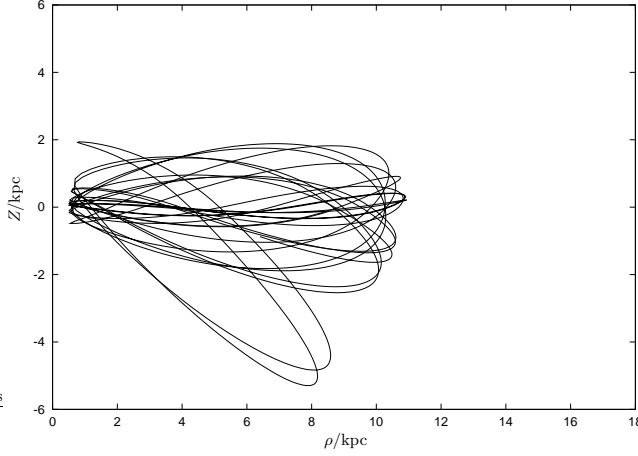


**Fig. 10.** Orbit of WD 0252–350, a halo white dwarf

bits like the halo main-sequence star HD 194598 (Fig. 11) are also members of the halo population. The white dwarfs WD 1448+077 and WD 1524–749 belong to this population.

To detect thick disk white dwarfs first all stars either situated outside the  $2\sigma$ -limit in the  $U$ - $V$ -diagram or in

Region 2 or 3 in the  $J_Z$ - $e$ -diagram are selected as thick disk candidates. According to these criteria 13 white dwarfs of our sample qualify.

In a second step each candidate is assigned a classification value  $c$ .  $c$  is defined as the sum of the individual values  $c_{UV}$ ,  $c_{Jze}$  and  $c_{orb}$  corresponding to the three different criteria: position in  $U$ - $V$ -diagram, position in  $J_Z$ - $e$ -diagram and orbit.

We assign  $c_{UV} = +1$  to a star outside the  $2\sigma$ -limit in the  $U$ - $V$ -diagram, whereas one inside the  $2\sigma$ -limit gets  $c_{UV} = -1$ . The different regions in the  $J_Z$ - $e$ -diagram are characterised by  $c_{Jze} = -1$  for Region 1, 0 for Region 3 and +1 for Region 2. The third classification value  $c_{orb}$  describes the orbits:  $c = -1$  for orbits of thin disk type and  $c = +1$  for orbits of thick disk type.

Then the sum  $c = c_{UV} + c_{Jze} + c_{orb}$  is computed. Stars with  $c = +3$  or  $c = +2$  are considered as bona fide thick disk members, those with  $c = +1$  as probable thick disk members. If  $c \leq 0$ , the star is classified as belonging to the thin disk. As we have selected halo members beforehand this classification scheme is not applied to halo stars.

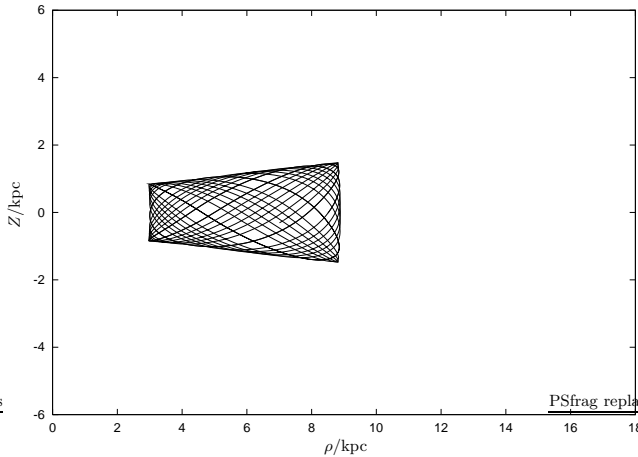


**Fig. 13.** Orbit of HD 221830, a thick disk main-sequence star

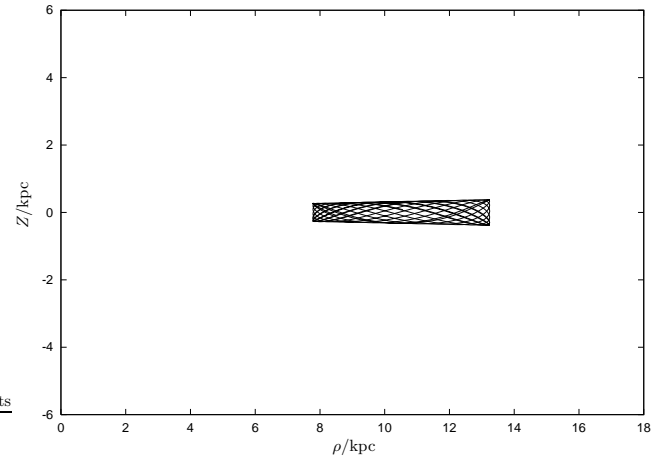


**Fig. 16.** Orbit of WD 0013-241, a thick disk white dwarf

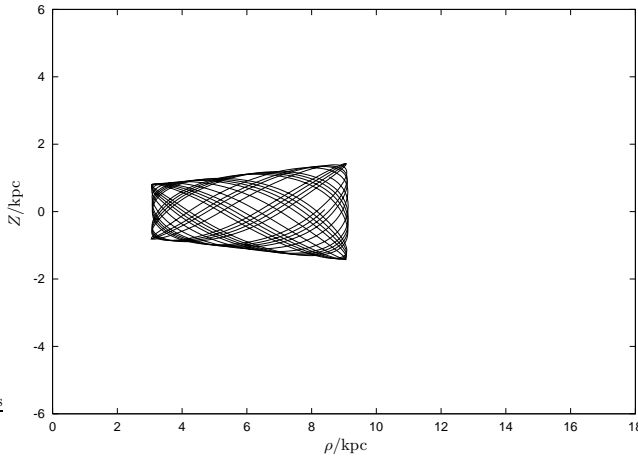


**Fig. 14.** Orbit of WD 1426-276, a thick disk white dwarf

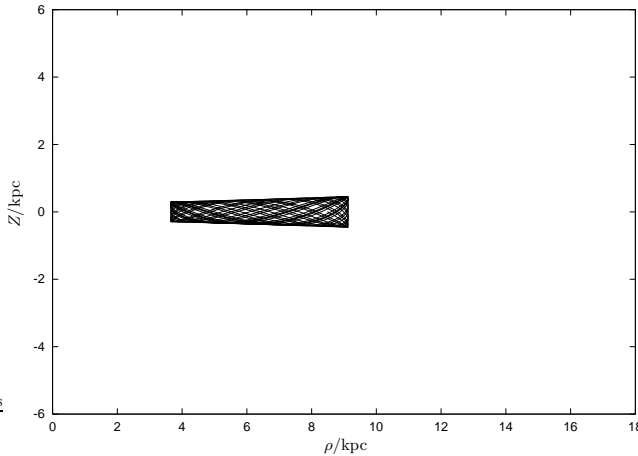


**Fig. 15.** Orbit of HD 165401, a thick disk main-sequence star

In Table 3 the individual and combined classification values for the thick disk candidates are listed. Applying our classification criteria we end up with nine bona fide and three probable thick disk white dwarfs. The total

number of white dwarfs belonging to the thick disk population is twelve.

### 5.1. Consistency check for classification criteria

In this section we perform a consistency check of our classification scheme. This is done by applying our kinematic classification criteria to our calibration main-sequence sample.

17 main-sequence stars are known to belong to the thick disk because of their abundance levels. For reasons mentioned above we exclude the star HD 184499 where kinematic and chemical criteria suggest different population memberships. Hence our total number of thick disk main-sequence stars is 16. Ten of them have a classification value  $c$  of +3 or +2 and are classified as bona fide thick disk stars. Five of them with  $c = +1$  are probable thick disk members. Only one of them has  $c = 0$  and is thus misclassified as thin disk star. Thus 15 out of 16 thick disk stars are identified correctly. This corresponds to a detection efficiency for thick disk members of about 94%. In addition to those 15 stars two thin disk main-sequence star also qualify as thick disk candidates because they lie outside the  $2\sigma$ -limit. One is classified as probable ( $c = +1$ ), the other as bona fide ( $c = +2$ ) thick disk member. Therefore both are misidentified as thick disk stars. The total number of stars classified as thick disk is 17 including two stars which really belong to the thin disk. So the contamination with thin disk stars is only about 12%.

We can therefore conclude that our selection criteria are very efficient in detecting thick disk stars while the contamination with thin disk stars is at an acceptable level.

### 5.2. The effects of setting $v_{\text{rad}} = 0$

All but two previous kinematic investigations on white dwarfs (Silvestri et al. 2001, 2002) assumed  $v_{\text{rad}} = 0$  (or  $W = 0$ ) simply because no radial velocity information was

available. We test the effects of this assumption by setting  $v_{\text{rad}}$  arbitrarily to zero for all stars in our sample.

First we compare the  $U$ - $V$ -velocity diagrams. In Fig. 17 the values for  $v_{\text{rad}} \neq 0$  are indicated by asterisks and those for  $v_{\text{rad}} = 0$  by open squares. As can be seen setting  $v_{\text{rad}} = 0$  generally increases both the  $U$  and  $V$  components. The number of white dwarfs outside the  $2\sigma$ -limit is reduced from 14 (for  $v_{\text{rad}} \neq 0$ ) to twelve (for  $v_{\text{rad}} = 0$ ). Four stars among them are far outside the  $2\sigma$ -limit. Those are the halo white dwarfs WD 0252–350, WD 2351–368, WD 1448+077 and WD 1524–749. The star that is affected most is WD 1524–749. Its value of  $V$  changes from  $-167 \text{ km s}^{-1}$  to  $-35 \text{ km s}^{-1}$ . This is not astonishing, as WD 1524–749 has a high radial velocity. The white dwarf WD 0252–350 is shifted closer to the  $2\sigma$ -border in  $V$ -direction.

Secondly we consider the  $J_Z$ - $e$ -diagram (Fig. 18). All four halo white dwarfs remain in Region 4. But the eccentricity of WD 0252–350 is reduced from 0.9 to 0.81 so that it gets closer to Region 2. WD 1524–749 shows a large shift as well, its eccentricity increases from 0.49 to 0.95 and its value of  $J_Z$  increases. This indicates that the orbit is changed from retrograde to prograde. For the other regions we note that the eccentricity decreases for nearly all stars. In consequence only five of the seven white dwarfs originally in Region 2 stay there whereas two are shifted to Region 1. Instead of five only four white dwarfs can now be found in Region 3.

Adopting the definition of a thick disk candidate (situated outside the  $2\sigma$ -limit in the  $U$ - $V$ -diagram or in Region 2 or 3 in the  $J_Z$ - $e$ -diagram) now twelve white dwarfs qualify whereas it have been 13 for for  $v_{\text{rad}} \neq 0$ .

Last we investigate the effect on the orbits. Again the former halo stars are affected strongly. The orbit of WD 1524–749 (Fig. 19) changes from a retrograde halo orbit to a typical halo orbit with very high extensions in  $\rho$  and  $Z$ . The shape of the orbit of WD 0252–350 (Fig. 20) is also altered. On the other hand for the thick disk candidates the effects on the orbits are small. Only for one white dwarf the orbit changes from thick disk to thin disk like.

Applying our classification scheme in Sect. 5 to the twelve thick disk candidates, ten of them pass the criteria for thick disk stars. Five with  $c \leq 2$  are classified as bona fide and five with  $c = 1$  as probable thick disk white dwarfs. The fact that we do only loose two of the twelve candidates to the thin disk is due to the robustness of the orbits to setting  $v_{\text{rad}} = 0$ . However the number of white dwarfs passing the criteria for thick disk candidates is reduced from 13 to ten stars, which is a loss of 23%. Though the eccentricities and the orbits of some halo members are altered they are still identified correctly as halo stars.

Silvestri et al. (2002) stated that setting  $v_{\text{rad}} = 0$  has only very small effects on the kinematics of white dwarfs. That may be true compared to setting  $W = 0 \text{ km s}^{-1}$  but we have demonstrated here that the effects are not negligible. Generally setting  $v_{\text{rad}} = 0$  can lead to an underestimate of the fraction of thick disk white dwarfs.

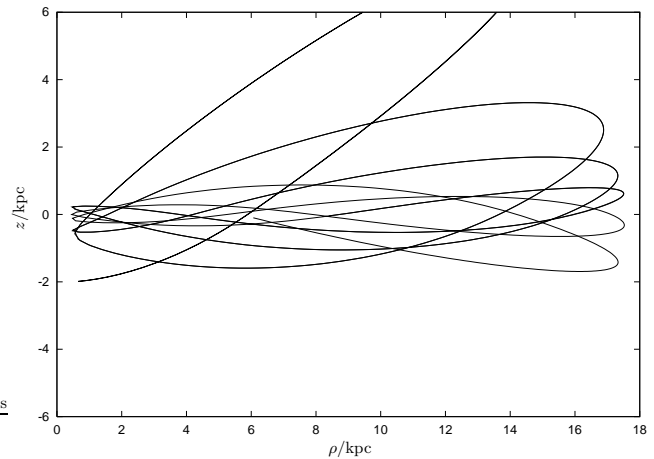


Fig. 19. Orbit of WD 1524–749 for  $v_{\text{rad}} = 0$

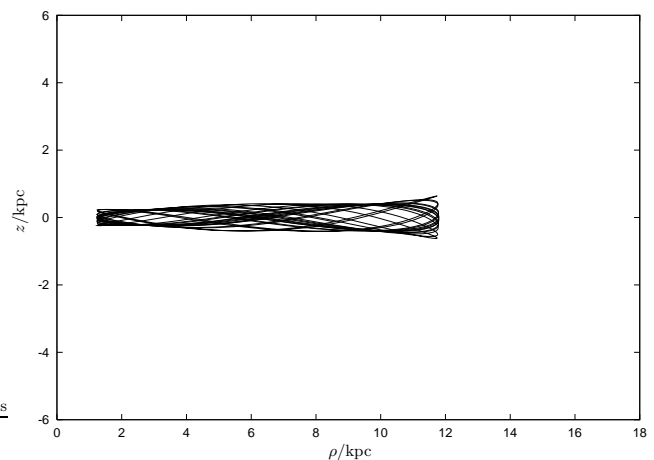


Fig. 20. Orbit of WD 0252–350 for  $v_{\text{rad}} = 0$

Misidentifications between thin and thick disk stars can occur and halo white dwarfs on retrograde orbits can appear to be on prograde ones. This should be kept in mind when dealing with samples for which radial velocities are not available.

## 6. Discussion

We have applied new sophisticated methods to kinematically analyse a sample of 107 DA white dwarfs from the SPY project. An error propagation method based on a Monte-Carlo technique was presented. It has been demonstrated that considering only the classical  $U$ - $V$ -diagram is not sufficient for deciding on population membership. In addition it is necessary to take the  $J_Z$ - $e$ -diagram and Galactic orbits into account. A quantitative method was developed for combining the three different classification criteria for thick disk white dwarfs. With a consistency check we have demonstrated that our detection rate for thick disk stars is very high (93%) with a contamination rate by thin disk stars of only 12%.

Four of our white dwarfs prove to be halo members, i.e. a fraction of 4%. Two of them are on retrograde or-

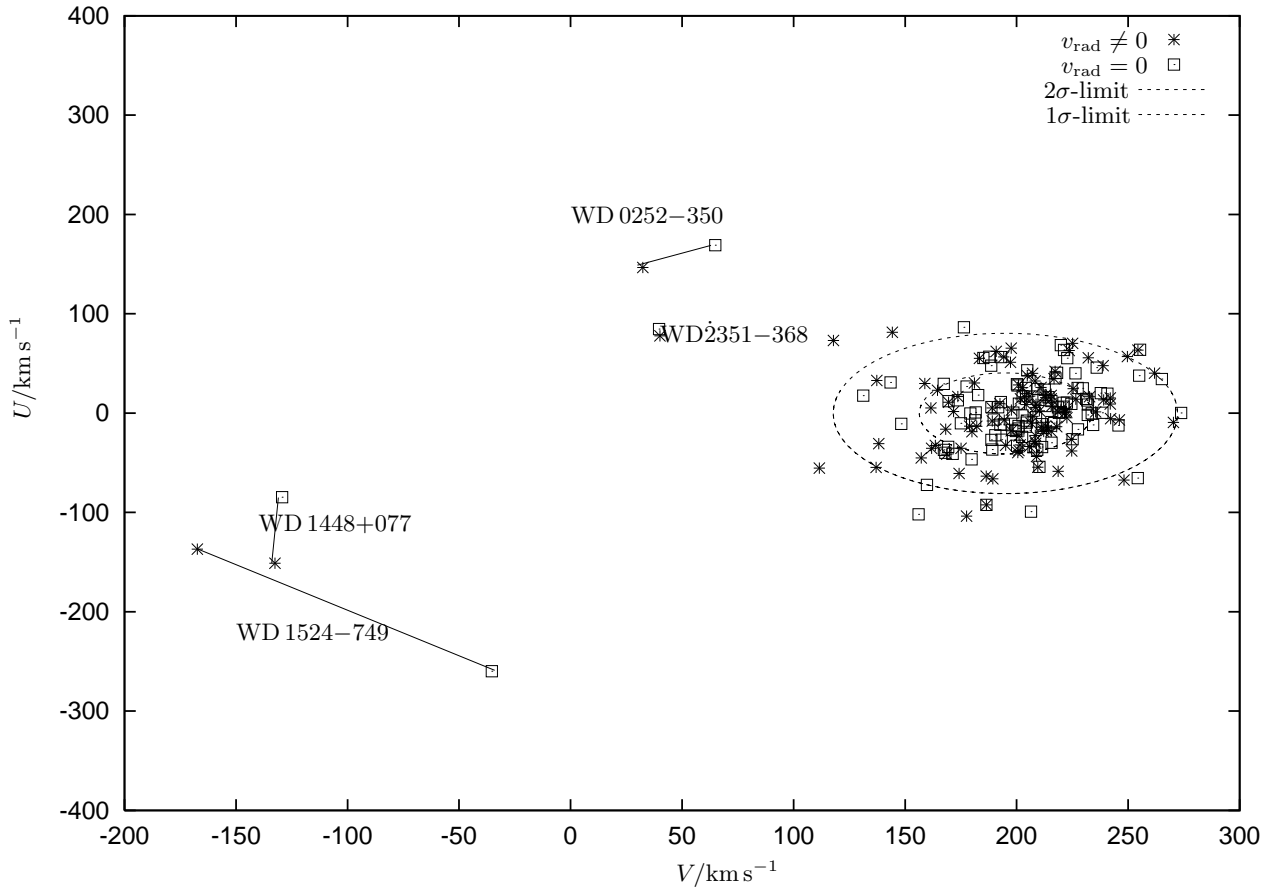


**Fig. 17.** Effect of setting  $v_{\text{rad}} = 0$  in the  $U$ - $V$ -diagram, the change in position of the halo white dwarfs is indicated by lines

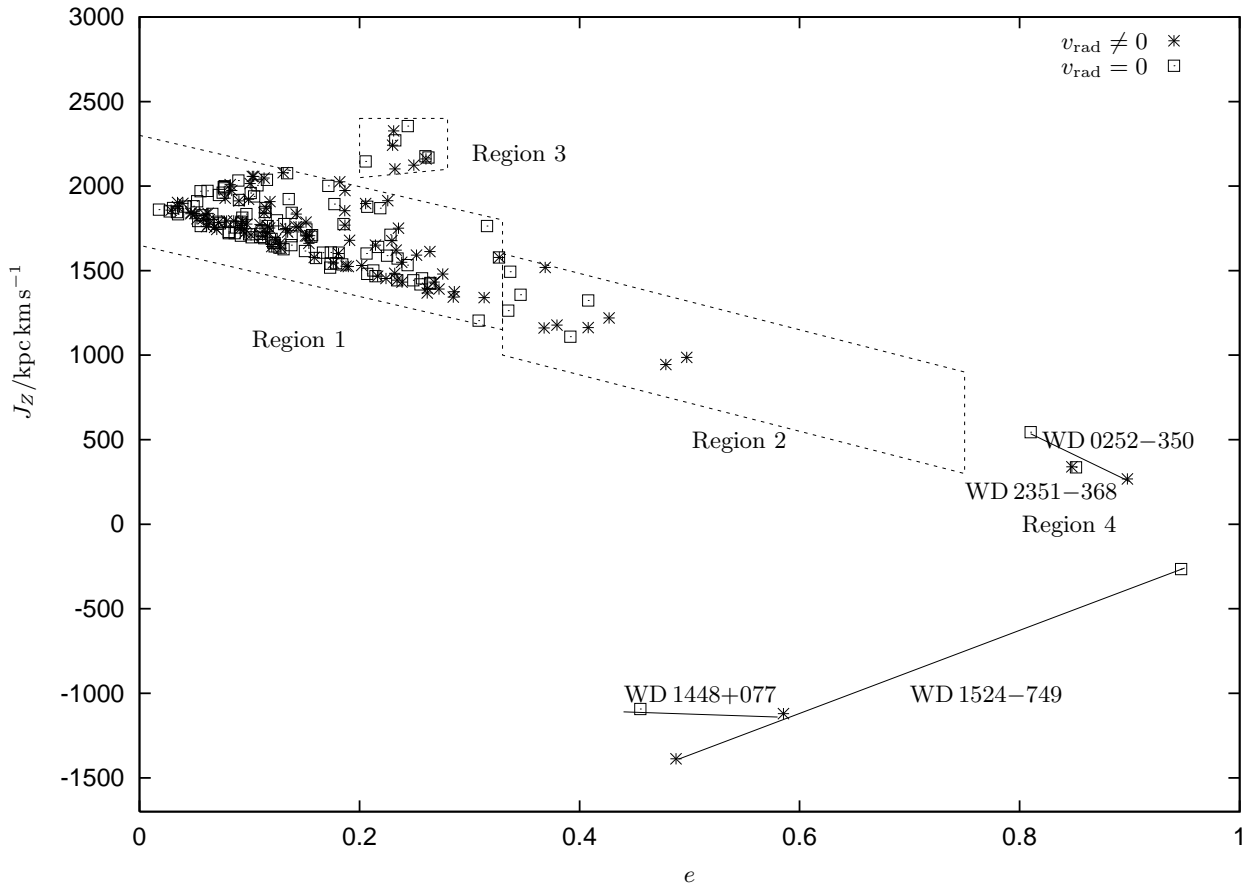


**Fig. 18.** Effect of setting  $v_{\text{rad}} = 0$  in the  $J_z$ - $e$ -diagram, the change in position of the halo white dwarfs is indicated by lines

bits. This percentage compares well with the results of Sion et al. (1988), who identified about 5% of their sample as halo white dwarfs. Liebert et al. (1989), on the other hand obtained a percentage of 14% halo white dwarfs by classifying all stars that exceed a certain value of tangential velocity as halo members. When comparing those samples with ours it has to be kept in mind that our selection criteria are finer and permit a separation of thick disk and halo. Therefore a part of the white dwarfs classified as halo by Sion et al. (1988) and Liebert et al. (1989) could belong to the thick disk instead. Furthermore both samples suffer from the lack of radial velocities.

Our sample does not confirm the results of Oppenheimer et al. (2001) who claim that halo white dwarfs constitute an important fraction of the dark matter in the Galaxy.

However, it has to be taken into account that our sample is biased towards high temperatures, whereas Oppenheimer et al. (2001) analyse cool white dwarfs. The first set of objects observed by SPY and analysed by Koester et al. (2001) was dominated by relatively hot white dwarfs (mean temperature of the Koester et al. (2001) sample: 21 700 K) selected from the Hamburg/ESO survey (Christlieb et al. 2001) and the white dwarf catalogue of McCook & Sion (1999).

Nine white dwarfs in our sample have been classified as bona-fide thick disk and three as probable thick disk. The combined total corresponds to a fraction of 11% thick disk white dwarfs in our local sample.

This value is compatible with the one of Silvestri et al. (2002). Our fraction of 11% thick disk white dwarfs, however, is somewhat smaller than that of Fuhrmann (2000) (<http://www.xray.mpe.mpg.de/fuhrmann/>) who predicted a fraction of 17% thick disk white dwarfs. The differences are possibly caused by the bias mentioned above. We cannot state an over-representation of white dwarfs compared to low mass main-sequence stars which would require a truncated initial mass function as suggested by Favata et al. (1997).

To discuss the kinematic parameters of our twelve thick disk white dwarfs we calculate the mean value and standard deviation of the three velocity components. The results can be found in Table 4. Those values are larger than those from Chiba & Beers (2000) who analysed the kinematics of 1203 solar-neighbourhood stars with metal abundances  $[\text{Fe}/\text{H}] \leq -0.6$ . This difference may be due to our stringent selection criteria. The mean eccentricity has a value of  $\langle e \rangle = 0.35$ , the mean  $z$ -component of angular momentum is  $\langle J_z \rangle = 1532 \text{ kpc km s}^{-1}$ .

Other interesting issues are the masses and cooling ages of our halo and thick disk white dwarfs. Masses of the white dwarfs are derived from effective temperatures and surface gravities by Koester et al. (2001) using the mass-radius relation from Wood (1995)'s white dwarf cooling tracks. In addition we calculated masses with another mass-radius relation from Blöcker et al. (1997), which is based on full evolutionary calculations.

Results are listed in Table 5 (thick disk white dwarfs) and Table 6 (halo white dwarfs) for both mass-radius relations.  $M_W$ ,  $M_B$  denote masses derived from Wood (1995) and Blöcker et al. (1997), respectively.

In the second column the number of spectra available is listed because we cannot rule out the possibility that stars without a second spectrum are spectroscopic binaries. All but one star in the halo/thick disk samples have  $T_{\text{eff}}$  above 13 000 K and are thus relatively hot and have a low cooling age ( $< 1 \text{ Gyr}$ ). Their typical mass is around  $0.5 \text{ M}_{\odot}$ . Only the halo star WD 0252–350 has a rather low mass indicating that it does not possess a CO- but a He-core instead. Generally our halo and thick disk white dwarfs are hot and have low masses. Exception to the rule is the thick disk star, WD 1334–678, which is cool ( $T_{\text{eff}} = 8958 \text{ K}$ ) and more massive,  $0.61 \text{ M}_{\odot}$ . The low masses and high temperatures of the majority of the halo and thick disk white dwarfs are in line with the assumption that these white dwarfs evolved from an old population of long-lived low mass stars. Their precursors did not yet have time to cool down to low temperatures. Since WD 1334–678 is more massive and cooler its origin may be different to that of the other thick disk stars. We speculate that this star might have been born in a binary system in the thin disk and been ejected thereafter from it (run-away star). A possible ejection mechanism would be e.g. a supernova explosion of the primary releasing the secondary at high velocity (Davies et al. 2002).

The question whether thick disk white dwarfs contribute significantly to the total mass of the Galaxy is of great importance to clarify the dark matter problem. We can estimate this contribution from our results derived above. To derive the densities of thin disk and thick disk white dwarfs we use the  $1/V_{\text{max}}$  method (Schmidt 1968). First we calculate the maximum distance  $d_{\text{max}}$  at which a white dwarf would still be included in our sample corresponding to  $B_{\text{max}} = 16.5$  for the stars with given  $B$ -magnitude or  $V_{\text{max}} = 16.5$  for the stars with given  $V$ -magnitude in Koester et al. (2001). The maximum, density-weighted volume  $V_{\text{max}}$  is then computed according to the following equation (Green 1980):

$$V_{\text{max}} = \int_0^{d_{\text{max}}} e^{-\frac{l}{l_0}} e^{-\frac{h}{h_0}} dV \quad (1)$$

where  $l_0$  and  $h_0$  are the scale lengths and heights for the white dwarfs classified as thin and thick disk members, respectively. For the thick disk we adopt the values of Ojha (2001): scale length  $l_{0,\text{thick}} = 3.7 \text{ kpc}$ , scale height  $h_{0,\text{thick}} = 0.86 \text{ kpc}$ . For the thin disk the corresponding scale length is  $l_{0,\text{thin}} = 2.8 \text{ kpc}$  (Ojha 2001) and the scale height is  $h_{0,\text{thin}} = 0.25 \text{ kpc}$  (Kuijken & Gilmore 1989; Kroupa 1992; Haywood et al. 1997). As over half of our sample stars possess distances exceeding 100 pc the assumption that  $d$  is small compared to the scale height is not valid. Thus  $V_{\text{max}}$  cannot be computed by the simple equation  $V_{\text{max}} = \frac{4}{3} \pi d_{\text{max}}^3$ .

To check the uniformity of the sample the mean value  $\left\langle \frac{V}{V_{\max}} \right\rangle$  is calculated. It is found to be 0.4 which is less than the 0.5 expected for a uniform, spherical distribution. Nevertheless, even a complete sample, if selected from a population with a nonuniform space-distribution such a disk system, will produce  $\left\langle \frac{V}{V_{\max}} \right\rangle < 0.5$  (Green 1980). For a disk-like structure with small scale height we evaluated  $\left\langle \frac{V}{V_{\max}} \right\rangle = 0.4$ .

The white dwarf density of a given population is:

$$\rho = \sum_i \frac{1}{V_{\max,i}}. \quad (2)$$

For the thick disk density we sum over all 12 thick disk stars, for the thin disk density over all 91 thin disk stars. To obtain the true density this sum would still have to be multiplied by the fraction of the sky  $\Omega$  covered by our observations. However, it is not necessary to know  $\Omega$ , which is difficult to estimate in our case since we are only interested in the fraction of mass contained in thick disk white dwarfs versus thin disk white dwarfs and  $\Omega$  cancels out in this fraction.

In following we describe how to obtain the mass fraction from the densities. The probability to find a star in a given volume is:

$$p(\mathbf{r}) = C e^{-\frac{l}{l_0}} e^{-\frac{h}{h_0}}. \quad (3)$$

We find  $C$  by the condition that the probability has to be normalised:

$$\int_0^\infty p(\mathbf{r}) dV \stackrel{!}{=} 1 \Rightarrow C = \frac{1}{\int_0^\infty e^{-\frac{l}{l_0}} e^{-\frac{h}{h_0}} dV}. \quad (4)$$

The connection between  $V_{\max}$  and  $p(\mathbf{r})$  is obtained by multiplying  $V_{\max}$  with  $C$ :

$$C \cdot V_{\max} = \int_0^{d_{\max}} p(\mathbf{r}) dV. \quad (5)$$

The number density  $N(\mathbf{r})$  is given by  $N(\mathbf{r}) = N_0 p(\mathbf{r})$ .

We now consider that we have one star  $i$  in the volume  $V_{\max,i}$ .

$$\begin{aligned} 1 &\stackrel{!}{=} \int_0^{d_{\max}} N(\mathbf{r}) dV \\ &= \int_0^{d_{\max}} N_{0,i} p(\mathbf{r}) dV \\ &= \int_0^{d_{\max}} N_{0,i} C e^{-\frac{l}{l_0}} e^{-\frac{h}{h_0}} dV \end{aligned} \quad (6)$$

$$\Rightarrow N_{0,i} = \frac{1}{C V_{\max,i}}. \quad (7)$$

By summing over all twelve thick disk white dwarfs the number of thick disk stars in the whole Galaxy can be extrapolated:

$$N_{0,\text{thick}} = \sum_{i=1}^{12} N_{0,i}$$

$$\begin{aligned} &= \frac{1}{C_{\text{thick}}} \sum_i \frac{1}{V_{\max,i}} \\ &= \int_0^\infty e^{-\frac{l}{l_0,\text{thick}}} e^{-\frac{h}{h_0,\text{thick}}} dV \sum_i \frac{1}{V_{\max,i}}. \end{aligned} \quad (8)$$

The same can be done for the 91 thin disk white dwarfs. Finally we obtain the mass fraction of thick disk versus thin disk white dwarfs by

$$\frac{M_{\text{thick}}}{M_{\text{thin}}} = \frac{N_{0,\text{thick}} \langle M_{\text{thick}} \rangle}{N_{0,\text{thin}} \langle M_{\text{thin}} \rangle} \quad (9)$$

with  $\langle M_{\text{thick}} \rangle$  and  $\langle M_{\text{thin}} \rangle$  being the mean mass of the thick and thin disk white dwarfs, respectively. Assuming  $\langle M_{\text{thick}} \rangle = \langle M_{\text{thin}} \rangle$  yields  $\frac{M_{\text{thick}}}{M_{\text{thin}}} = 0.15 \pm 0.32$ . The error of 216% was derived using linear error propagation. Its large value results from the poor statistics of the relatively small thick disk sample. Nevertheless we can conclude within the  $1\sigma$ -level that the total mass of thick disk white dwarfs is less than one half of the total mass of thin disk white dwarfs. Therefore the mass contribution of the thick disk white dwarfs cannot be neglected, but it is not sufficient to account for the missing dark matter.

## 7. Conclusions

We have demonstrated how a combination of sophisticated kinematic analysis tools can provide a distinction of halo, thick disk and thin disk white dwarfs. We have identified a fraction of 4% halo and 11% thick disk white dwarfs. No indications for the existence of a white dwarf dark halo or a truncated thick disk IMF function have been found. Most of our thick disk and halo white dwarfs are hot and possess low masses. Our results do suggest that the mass present in halo and thick disk white dwarfs is not sufficient to explain the missing mass of the Galaxy. But to draw definite conclusions more data is needed. Our goal is to extend this kinematic analysis to all 1 000 white dwarfs from the SPY project in order to have a large data base to decide on population membership of white dwarfs and their implications for the mass and evolution of the Galaxy.

*Acknowledgements.* E.-M. P. acknowledges support by the Deutsche Forschungsgemeinschaft (grant Na365/2-1). E.-M. P. also wishes to express gratitude to the Studienstiftung des Deutschen Volkes for a grant. Without their travel support it would not have been possible to attend the White Dwarf Workshop 2002. Thanks go to J. Pauli for interesting and fruitful discussions. M. Altmann acknowledges support from the DLR 50 QD 0102. We are also grateful for DSS images based on photographic data obtained from the UK Schmidt Telescope. The UK Schmidt Telescope was operated by the Royal Observatory Edinburgh, with funding from the UK Science and Engineering Research Council, until 1988 June, and thereafter by the Anglo-Australian Observatory. Original plate material is copyright of the Royal Observatory Edinburgh and the Anglo-Australian Observatory. The plates were processed into the present compressed digital form with their permission. The Digitized Sky Survey was produced at the Space

Telescope Science Institute under US Government grant NAG W-2166.

## References

Alcock, C., Allsmann, R., Alves, D. R., et al. 2000, *ApJ*, 542, 227

Allen, C. & Santillan, A. 1991, *Rev. Mex. Astron. Astrofis.*, 22, 255

Altmann, M. 2002, PhD thesis, Universität Bonn

Barbier-Brossat, M., Petit, M., & Figon, P. 1994, *A&AS*, 108, 603

Bertin, E. & Arnouts, S. 1996, *A&AS*, 117, 393

Blöcker, T., Herwig, F., Driebe, T., Bramkamp, H., & Schönberner, D. 1997, in *Proceedings of the 10th European Workshop on White Dwarfs*, ed. J. Isern, M. Hernanz, & E. Garcia-Berro, *Astrophysics and Space Science Library*, Vol. 214 (Dordrecht: Kluwer Academic Publishers), p. 57

Chiba, M. & Beers, T. C. 2000, *AJ*, 119, 2843

Christlieb, N., Wisotzki, L., Reimers, D., et al. 2001, *A&A*, 366, 898

Davies, M. B., King, A., & Ritter, H. 2002, *MNRAS*, 333, 463

Dehnen, W. & Binney, J. J. 1998, *MNRAS*, 298, 387

Edvardsson, B., Andersen, J., Gustafsson, B., et al. 1993, *A&A*, 275, 101

Favata, F., Micela, G., & Sciortino, S. 1997, *A&A*, 323, 809

Flynn, C., Sommer-Larsen, J., & Christensen, P. R. 1996, *MNRAS*, 281, 1027

Fuhrmann, K. 1998, *A&A*, 338, 161

Garcia-Berro, E., Torres, S., & Isern, J. 1999, in *Proceedings of the 11th European Workshop on White Dwarfs*, ed. J.-E. Solheim & E. G. Meistas, *ASP Conf. Ser.* 169, *Astronomical Society of the Pacific*, p. 69

Geffert, M., Klemola, A. R., Hiesgen, M., & Schmoll, J. 1997, *A&AS*, 124, 357

Gershenfeld, N. 1999, *The Nature of Mathematical Modelling* (Cambridge: Cambridge University Press)

Green, R. F. 1980, *ApJ*, 238, 685

Green, R. F., Schmidt, M., & Liebert, J. 1986, *ApJS*, 61, 305

Hagen, H.-J., Groote, D., Engels, D., & Reimers, D. 1995, *A&AS*, 111, 195

Haywood, M., Robin, A. C., & Creze, M. 1997, *A&A*, 320, 440

Homeier, D., Koester, D., Hagen, H.-J., et al. 1998, *A&A*, 338, 563

Kerr, F. J. & Lynden-Bell, D. 1986, *MNRAS*, 221, 1023

Kilkenny, D., O'Donoghue, D., Koen, C., Stobie, R. S., & Chen, A. 1997, *MNRAS*, 287, 867

Koester, D., Napiwotzki, R., Christlieb, N., et al. 2001, *A&A*, 378, 556

Kroupa, P. 1992, in *Complementary approaches to Double and Multiple Star Research*, ed. H. A. McAlister & W. I. Hartkopf, *ASP Conf. Ser.* 32, *Astronomical Society of the Pacific*, p. 228

Kuijken, K. & Gilmore, G. 1989, *MNRAS*, 239, 571

Lamontagne, R., Demers, S., Wesemael, F., Fontaine, G., & Irwin, M. J. 2000, *AJ*, 119, 241

Liebert, J., Dahn, C. C., & Monet, D. G. 1989, in *Proceedings of IAU Colloquium 114th* (Hanover, NH: Springer-Verlag), p. 15

Luyten, W. J. 1979, *LHS catalogue* (Minneapolis: University of Minnesota Press)

McCook, G. P. & Sion, E. M. 1987, *ApJS*, 65, 603

—. 1999, *ApJS*, 121, 1

Monet, D., Bird, A., Canzian, B., et al. 1998, *VizieR On-line Catalog*: I/252

Napiwotzki, R., Christlieb, N., Drechsel, H., et al. 2001, *AN*, 121, 503

Odenkirchen, M. & Brosche, P. 1992, *AN*, 313, 69

Ojha, D. K. 2001, *MNRAS*, 322, 426

Oppenheimer, B. R., Hambly, N. C., Digby, A. P., Hodgkin, S. T., & Saumon, D. 2001, *Sci*, 292, 698

Ostriker, J. P. & Peebles, P. J. E. 1973, *ApJ*, 186, 467

Reid, I. N., Kailash, K. C., & Hawley, S. L. 2001, *ApJ*, 559, 942

Rubin, V., Ford, W. K. J., & Thonnard, N. 1978, *ApJ*, 225, 107

Schmidt, M. 1968, *ApJ*, 151, 393

Silvestri, N. M., Oswalt, T. D., & Hawley, S. L. 2002, *AJ*, 124, 1118

Silvestri, N. M., Oswalt, T. D., Wood, M. A., et al. 2001, *AJ*, 121, 503

Sion, E. M., Fritz, M. L., McMullin, J. P., & Lallo, M. D. 1988, *AJ*, 96, 251

Stetson, P. B. 1992, in *ASP Conf. Ser.* 25: *Astronomical Data Analysis Software and Systems I*, Vol. 1, 297

Wisotzki, L., Christlieb, N., Bade, N., et al. 2000, *A&A*, 358, 77

Wisotzki, L., Koehler, T., Groote, D., & Reimers, D. 1996, *A&AS*, 115, 227

Wood, M. A. 1995, in *White Dwarfs*, *Proceedings of the 11th European Workshop on White Dwarfs Held at Kiel, Germany, 29 August-1 September 1994*, ed. D. Koester & K. Werner, *ASP Conf. Ser.* 169, *Astronomical Society of the Pacific*, p. 348

Zacharias, N., Urban, S. E., Zacharias, M. I., et al. 2000, *AJ*, 120, 2131

**Table 1.** Radial velocities (corrected for gravitational redshift), proper motion components and spectroscopic distances (with errors) of the white dwarfs

| star         | spectra | $v_{\text{rad}}$<br>km s $^{-1}$ | $\mu_{\alpha} \cos \delta$<br>mas yr $^{-1}$ | $\mu_{\delta}$<br>mas yr $^{-1}$ | $d$<br>pc | $\log d$<br>pc |
|--------------|---------|----------------------------------|--|----------------------------------|-----------|----------------|
| HE 0348–4445 | 2       | 26.5±3.9                         | −16±18                                       | 29±18                            | 119.2     | 2.08±0.03      |
| HE 0358–5127 | 2       | 12.9±3.6                         | 4±17   | 2±17                             | 120.5     | 2.08±0.03      |
| HE 0403–4129 | 2       | 4.7±4.1                          | −17±19                                       | −16±19                           | 146.0     | 2.16±0.03      |
| HE 0409–5154 | 1       | 46.2±3.6                         | 42±17  | −132±17                          | 147.0     | 2.17±0.03      |
| HE 0507–1855 | 2       | 17.8±4.9                         | −20±17                                       | 0±17                             | 116.0     | 2.06±0.03      |
| HE 0532–5605 | 1       | 15.2±5.2                         | 31±18  | 1±18                             | 52.2      | 1.72±0.03      |
| HE 1012–0049 | 1       | −3.7±3.9                         | −13±30                                       | 26±30                            | 99.7      | 2.00±0.02      |
| HE 1053–0914 | 1       | 7.5±3.4                          | −14±28                                       | −15±28                           | 195.3     | 2.29±0.02      |
| HE 1117–0222 | 1       | 15.2±3.2                         | −132±11                                      | −10±11                           | 38.3      | 1.58±0.03      |
| HE 1124+0144 | 2       | 54.6±3.1                         | −175±27                                      | 46±27                            | 133.1     | 2.12±0.03      |
| HE 1152–1244 | 1       | 12.4±2.7                         | −19±25                                       | −47±25                           | 88.7      | 1.95±0.02      |
| HE 1215+0227 | 2       | 2.0±12.0                         | −19±20                                       | −13±20                           | 377.6     | 2.58±0.04      |
| HE 1225+0038 | 2       | −24.0±3.7                        | −52±10                                       | 98±10                            | 29.0      | 1.46±0.03      |
| HE 1252–0202 | 2       | −2.1±3.8                         | −12±11                                       | −43±11                           | 124.0     | 2.09±0.02      |
| HE 1307–0059 | 2       | 27.2±3.4                         | −82±46                                       | −61±46                           | 99.5      | 2.00±0.03      |
| HE 1310–0337 | 1       | 19.7±3.7                         | −47±20                                       | −8±20                            | 149.0     | 2.17±0.03      |
| HE 1315–1105 | 1       | −3.4±3.6                         | −141±21                                      | 12±21                            | 39.7      | 1.60±0.03      |
| HE 1326–0041 | 2       | 2.6±3.7                          | 34±16  | −42±16                           | 132.5     | 2.12±0.03      |
| HE 1328–0535 | 2       | 3.2±7.3                          | −20±20                                       | −15±20                           | 246.4     | 2.39±0.03      |
| HE 1335–0332 | 2       | 1.6±6.6                          | −57±25                                       | 12±25                            | 109.3     | 2.04±0.03      |
| HE 1413+0021 | 2       | −8.2±4.1                         | 49±18  | 19±18                            | 70.7      | 1.85±0.03      |
| HE 1441–0047 | 2       | −11.6±4.7                        | 32±17  | 4±17                             | 108.4     | 2.04±0.03      |
| HE 1518–0020 | 1       | 5.9±3.3                          | −98±21                                       | −113±21                          | 73.2      | 1.86±0.02      |
| HE 1518–0344 | 2       | −0.7±5.6                         | −31±29                                       | −23±29                           | 204.8     | 2.31±0.03      |
| HE 1522–0410 | 2       | −11.6±4.2                        | −7±29  | −7±29                            | 66.0      | 1.82±0.03      |
| WD 0000–186  | 2       | 5.2±3.4                          | −46±22                                       | −94±22                           | 111.4     | 2.05±0.05      |
| WD 0005–163  | 1       | −9.4±3.7                         | 169±22                                       | −56±22                           | 91.3      | 1.96±0.03      |
| WD 0011+000  | 2       | −12.0±3.6                        | 420±10                                       | −182±10                          | 36.5      | 1.56±0.03      |
| WD 0013–241  | 2       | −6.9±3.2                         | −149±17                                      | 2±17                             | 86.8      | 1.94±0.03      |
| WD 0016–220  | 2       | −6.4±2.8                         | −53±16                                       | −58±16                           | 68.3      | 1.83±0.03      |
| WD 0016–258  | 2       | 15.8±3.7                         | −12±17                                       | −64±17                           | 66.8      | 1.82±0.05      |
| WD 0102–142  | 1       | −2.9±3.5                         | 54±6   | 37±5                             | 122.6     | 2.09±0.05      |
| WD 0106–358  | 2       | 8.6±4.4                          | 1±15   | −56±15                           | 97.4      | 1.99±0.03      |
| WD 0108+143  | 1       | 13.1±6.5                         | 292±10                                       | −63±10                           | 37.0      | 1.57±0.06      |
| WD 0110–139  | 2       | 8.0±3.8                          | 3±5  | −20±5                            | 129.2     | 2.11±0.05      |
| WD 0124–257  | 2       | 10.5±3.5                         | 52±20  | −73±20                           | 129.4     | 2.11±0.05      |
| WD 0126+101  | 2       | −17.6±2.7                        | −146±16                                      | −382±16                          | 25.0      | 1.40±0.03      |
| WD 0129–205  | 2       | 33.6±3.6                         | 168±19                                       | 24±21                            | 63.7      | 1.80±0.05      |
| WD 0137–291  | 2       | 5.7±3.6                          | 53±20  | −5±20                            | 151.8     | 2.18±0.05      |
| WD 0138–236  | 2       | 26.0±7.1                         | 5±20   | −1±20                            | 298.9     | 2.48±0.06      |
| WD 0140–392  | 2       | 25.7±3.5                         | 141±16                                       | 68±16                            | 56.8      | 1.75±0.03      |
| WD 0151+017  | 2       | 40.7±3.0                         | 296±105                                      | 10±105                           | 54.2      | 1.73±0.03      |
| WD 0204–233  | 1       | 76.3±2.7                         | 185±79                                       | −116±79                          | 79.1      | 1.90±0.03      |
| WD 0205–304  | 1       | 57.3±3.1                         | 167±17                                       | −26±17                           | 93.6      | 1.97±0.03      |
| WD 0209+085  | 2       | 53.8±5.4                         | 78±11  | −20±11                           | 101.7     | 2.01±0.06      |
| WD 0216+143  | 1       | −9.3±3.4                         | −100±10                                      | 42±10                            | 89.6      | 1.95±0.03      |
| WD 0252–350  | 2       | 86.4±2.4                         | 36±19  | −343±19                          | 137.7     | 2.14±0.05      |
| WD 0339–035  | 1       | 50.9±3.3                         | 252±45                                       | 58±45                            | 54.9      | 1.74±0.03      |
| WD 0408–041  | 1       | −9.6±3.5                         | −6±170                                       | −103±170                         | 73.2      | 1.86±0.03      |
| WD 0416–550  | 2       | 19.6±3.6                         | 49±17  | 5±17                             | 226.1     | 2.35±0.05      |
| WD 0509–007  | 1       | 11.1±3.1                         | −73±10                                       | 61±10                            | 116.9     | 2.07±0.03      |
| WD 0911–076  | 2       | 34.1±3.2                         | −63±30                                       | 6±30                             | 121.5     | 2.08±0.03      |
| WD 0939–153  | 2       | 22.2±2.7                         | −35±23                                       | 42±23                            | 95.5      | 1.98±0.03      |
| WD 0951–155  | 2       | 7.7±3.0                          | −88±23                                       | 115±23                           | 121.0     | 2.08±0.02      |
| WD 0956+020  | 2       | 40.1±2.8                         | 45±20  | 5±20                             | 89.3      | 1.95±0.05      |

**Table 1.** Radial velocities (corrected for gravitational redshift), proper motion components and spectroscopic distances (with errors) of the white dwarfs  
continued from previous page

| star        | spectra | $v_{\text{rad}}$<br>km s $^{-1}$ | $\mu_{\alpha} \cos\delta$<br>mas yr $^{-1}$ | $\mu_{\delta}$<br>mas yr $^{-1}$ | $d$<br>pc | $\log d$<br>pc |
|-------------|---------|----------------------------------|---|----------------------------------|-----------|----------------|
| WD 1015–216 | 1       | −12.6±5.4                        | −13±18                                      | −21±18                           | 173.5     | 2.24±0.03      |
| WD 1020–207 | 1       | 56.3±2.9                         | −74±12                                      | −15±12                           | 83.2      | 1.92±0.03      |
| WD 1102–183 | 1       | 24.0±3.6                         | 135±19                                      | −73±19                           | 39.9      | 1.60±0.03      |
| WD 1122–324 | 1       | −19.9±3.2                        | −84±19                                      | 4±19                             | 127.6     | 2.11±0.03      |
| WD 1124–293 | 1       | −2.6±3.5                         | 225±23                                      | −286±23                          | 33.9      | 1.53±0.03      |
| WD 1126–222 | 1       | 32.5±3.4                         | −151±18                                     | −52±18                           | 93.3      | 1.97±0.03      |
| WD 1144–246 | 1       | −14.5±3.9                        | −30±19                                      | −14±19                           | 270.7     | 2.43±0.03      |
| WD 1150–153 | 1       | 1.7±3.4                          | −17±25                                      | −65±25                           | 84.6      | 1.93±0.03      |
| WD 1155–243 | 2       | 22.9±3.2                         | −75±18                                      | −107±18                          | 116.2     | 2.07±0.03      |
| WD 1159–098 | 2       | −7.3±6.3                         | −156±46                                     | −112±46                          | 33.0      | 1.52±0.03      |
| WD 1201–001 | 2       | 10.8±4.4                         | −153±54                                     | 29±54                            | 63.7      | 1.80±0.03      |
| WD 1204–322 | 1       | −12.0±3.4                        | −70±11                                      | −31±11                           | 103.0     | 2.01±0.03      |
| WD 1207–157 | 2       | −14.2±3.1                        | −60±25                                      | −18±25                           | 141.3     | 2.15±0.02      |
| WD 1244–125 | 1       | 2.7±3.0                          | −180±25                                     | −3±25                            | 48.6      | 1.69±0.03      |
| WD 1326–236 | 2       | −16.7±3.3                        | −49±17                                      | −14±17                           | 93.6      | 1.97±0.03      |
| WD 1334–678 | 1       | 28.9±3.9                         | −607±56                                     | −18±56                           | 37.1      | 1.57±0.03      |
| WD 1342–237 | 2       | 15.3±4.1                         | −20±17                                      | −2±17                            | 64.7      | 1.81±0.03      |
| WD 1344+106 | 1       | −60.2±4.1                        | −886±10                                     | −144±10                          | 18.2      | 1.26±0.03      |
| WD 1356–233 | 1       | −57.4±3.8                        | −324±19                                     | −50±19                           | 31.2      | 1.49±0.03      |
| WD 1401–147 | 2       | −13.6±3.5                        | −160±21                                     | −116±21                          | 59.3      | 1.77±0.03      |
| WD 1422+095 | 2       | −29.2±3.3                        | −211±10                                     | −147±10                          | 36.9      | 1.57±0.03      |
| WD 1426–276 | 2       | 56.8±2.6                         | −3±23                                       | −228±23                          | 123.4     | 2.09±0.03      |
| WD 1448+077 | 1       | −118.5±2.7                       | −816±11                                     | −454±11                          | 85.0      | 1.93±0.03      |
| WD 1457–086 | 2       | −6.1±3.5                         | 11±20                                       | −42±20                           | 118.6     | 2.07±0.03      |
| WD 1515–164 | 1       | 23.8±3.1                         | 105±27                                      | −10±27                           | 97.1      | 1.99±0.03      |
| WD 1524–749 | 2       | 187.2±3.0                        | −407±16                                     | −254±16                          | 165.5     | 2.22±0.03      |
| WD 1537–152 | 2       | −22.6±3.3                        | −84±38                                      | 17±38                            | 98.5      | 1.99±0.02      |
| WD 1555–089 | 2       | 44.0±3.9                         | −66±25                                      | −145±25                          | 58.5      | 1.77±0.03      |
| WD 1609+135 | 1       | 26.4±6.1                         | 17±10                                       | −537±10                          | 21.6      | 1.33±0.03      |
| WD 1636+057 | 2       | −8.4±6.9                         | −307±10                                     | −418±10                          | 24.9      | 1.40±0.03      |
| WD 1834–781 | 2       | 71.5±2.8                         | 130±16                                      | −313±16                          | 92.8      | 1.97±0.03      |
| WD 1952–206 | 2       | 18.0±2.9                         | 109±19                                      | −380±19                          | 60.7      | 1.78±0.03      |
| WD 1959+059 | 2       | −40.9±4.5                        | −120±10                                     | −110±10                          | 80.4      | 1.91±0.03      |
| WD 2007–219 | 2       | −55.9±3.6                        | 108±19                                      | −308±19                          | 25.5      | 1.41±0.03      |
| WD 2014–575 | 1       | 40.9±3.4                         | 69±19                                       | −39±19                           | 44.5      | 1.65±0.03      |
| WD 2139+115 | 1       | −0.6±3.1                         | 204±10                                      | −25±10                           | 98.9      | 2.00±0.03      |
| WD 2151–307 | 2       | 6.0±5.0                          | 37±17                                       | −12±17                           | 85.7      | 1.93±0.03      |
| WD 2254+126 | 2       | −10.6±4.2                        | 186±10                                      | 1±10                             | 63.0      | 1.80±0.05      |
| WD 2306+124 | 2       | 13.8±3.6                         | −7±10                                       | 23±10                            | 85.4      | 1.93±0.03      |
| WD 2311–260 | 2       | 25.7±6.8                         | 12±18                                       | −7±18                            | 434.9     | 2.64±0.04      |
| WD 2318–226 | 2       | 15.5±5.0                         | 6±18  | −51±18                           | 209.7     | 2.32±0.03      |
| WD 2322–181 | 2       | −0.3±3.2                         | 242±19                                      | 10±19                            | 101.0     | 2.00±0.05      |
| WD 2326+049 | 1       | 15.3±3.0                         | −412±10                                     | −263±10                          | 19.2      | 1.28±0.03      |
| WD 2329–332 | 2       | 13.1±3.7                         | 19±22                                       | 37±22                            | 157.5     | 2.20±0.05      |
| WD 2333–049 | 2       | 11.3±3.7                         | −193±37                                     | −124±37                          | 53.5      | 1.73±0.03      |
| WD 2333–165 | 1       | 47.5±2.6                         | 87±30                                       | −147±30                          | 31.8      | 1.50±0.03      |
| WD 2347–192 | 1       | 12.9±4.1                         | −46±19                                      | −8±19                            | 167.9     | 2.23±0.03      |
| WD 2348–244 | 2       | 36.5±3.5                         | −94±19                                      | −237±19                          | 49.7      | 1.70±0.03      |
| WD 2349–283 | 2       | 17.1±2.9                         | 44±17                                       | −62±17                           | 96.7      | 1.99±0.05      |
| WD 2350–248 | 2       | 10.8±5.5                         | −13±19                                      | 8±19                             | 99.9      | 2.00±0.05      |
| WD 2351–368 | 2       | −26.9±3.0                        | 33±17                                       | −680±17                          | 62.6      | 1.80±0.05      |
| WD 2354–151 | 1       | 7.3±3.6                          | −1±22                                       | −23±22                           | 278.9     | 2.45±0.05      |

**Table 2.** Kinematic parameters of the white dwarfs

| star         | $e$       | $J_z$<br>kpc km s $^{-1}$ | $U$<br>km s $^{-1}$ | $V$<br>km s $^{-1}$ | $W$<br>km s $^{-1}$ |
|--------------|-----------|---------------------------|---------------------|---------------------|---------------------|
| HE 0348–4445 | 0.04±0.02 | 1898±59                   | −4.6±8.0            | 222.6±6.9           | −20.9±6.1           |
| HE 0358–5127 | 0.05±0.02 | 1837±53                   | 7.4±7.8             | 215.8±6.2           | −1.5±5.6            |
| HE 0403–4129 | 0.10±0.03 | 1922±75                   | 24.6±10.6           | 225.3±8.8           | −4.5±7.5            |
| HE 0409–5154 | 0.43±0.03 | 1220±63                   | 81.3±10.4           | 144.3±7.4           | 9.4±7.1             |
| HE 0507–1855 | 0.03±0.02 | 1903±60                   | 0.8±6.4             | 221.9±6.9           | −10.9±6.9           |
| HE 0532–5605 | 0.06±0.02 | 1774±35                   | 9.1±3.6             | 208.7±4.2           | 5.3±3.9             |
| HE 1012–0049 | 0.08±0.03 | 2009±75                   | 1.3±10.6            | 235.4±8.8           | 6.7±8.6             |
| HE 1053–0914 | 0.10±0.05 | 1775±123                  | 5.7±20.0            | 208.4±14.4          | −0.5±14.9           |
| HE 1117–0222 | 0.07±0.01 | 1756±18                   | −10.1±1.9           | 206.5±2.1           | 9.9±2.4             |
| HE 1124+0144 | 0.37±0.04 | 1519±102                  | −103.8±15.1         | 177.6±12.0          | 30.3±7.9            |
| HE 1152–1244 | 0.10±0.03 | 1711±57                   | 14.4±8.2            | 201.7±6.7           | 1.9±6.1             |
| HE 1215+0227 | 0.18±0.09 | 1601±227                  | −7.8±28.8           | 189.1±26.8          | −5.2±15.6           |
| HE 1225+0038 | 0.10±0.01 | 2057±14                   | −5.5±1.4            | 242.1±1.7           | −8.9±2.7            |
| HE 1252–0202 | 0.10±0.02 | 1722±43                   | 16.5±5.2            | 203.5±5.0           | −7.0±3.8            |
| HE 1307–0059 | 0.22±0.07 | 1454±140                  | 1.6±16.8            | 171.7±16.5          | 19.7±9.1            |
| HE 1310–0337 | 0.12±0.05 | 1643±94                   | −7.0±11.3           | 194.4±11.1          | 23.8±6.6            |
| HE 1315–1105 | 0.05±0.01 | 1808±29                   | −12.9±3.5           | 213.0±3.4           | 8.5±3.1             |
| HE 1326–0041 | 0.14±0.02 | 1834±65                   | 42.0±8.0            | 217.3±7.7           | −5.7±4.7            |
| HE 1328–0535 | 0.13±0.06 | 1658±155                  | 3.0±17.8            | 197.7±18.5          | 3.0±11.7            |
| HE 1335–0332 | 0.07±0.03 | 1785±85                   | −14.1±9.9           | 211.1±10.0          | 16.9±7.5            |
| HE 1413+0021 | 0.11±0.02 | 2047±43                   | 15.3±4.7            | 242.0±5.1           | −2.4±4.0            |
| HE 1441–0047 | 0.10±0.03 | 2015±61                   | 13.3±6.2            | 239.0±7.3           | −8.2±5.2            |
| HE 1518–0020 | 0.22±0.03 | 1467±52                   | 16.7±4.7            | 173.6±6.1           | 12.3±4.6            |
| HE 1518–0344 | 0.16±0.09 | 1578±191                  | 5.3±15.7            | 189.0±22.9          | 11.1±17.3           |
| HE 1522–0410 | 0.03±0.02 | 1878±64                   | 2.0±5.4             | 222.2±7.6           | −0.3±6.0            |
| WD 0000–186  | 0.21±0.04 | 1650±82                   | 56.7±10.3           | 194.2±9.7           | −1.4±3.7            |
| WD 0005–163  | 0.27±0.03 | 1432±66                   | −41.4±7.8           | 168.7±7.8           | −1.0±3.5            |
| WD 0011+000  | 0.29±0.02 | 1376±30                   | −35.5±2.8           | 161.9±3.6           | −7.7±3.1            |
| WD 0013–241  | 0.26±0.02 | 2161±51                   | 63.5±6.2            | 254.4±6.0           | 22.5±2.7            |
| WD 0016–220  | 0.11±0.01 | 1842±34                   | 34.8±4.1            | 216.7±4.0           | 13.7±2.4            |
| WD 0016–258  | 0.09±0.02 | 1791±40                   | 25.8±4.6            | 210.9±4.7           | −8.9±3.1            |
| WD 0102–142  | 0.09±0.01 | 1913±20                   | −26.5±4.6           | 224.6±2.4           | 16.5±2.8            |
| WD 0106–358  | 0.12±0.02 | 1722±49                   | 25.6±5.6            | 202.7±5.8           | 2.5±3.6             |
| WD 0108+143  | 0.15±0.02 | 1661±41                   | −32.3±4.8           | 195.1±4.9           | −6.1±4.1            |
| WD 0110–139  | 0.05±0.01 | 1838±23                   | 14.5±2.6            | 215.5±2.8           | −3.3±3.1            |
| WD 0124–257  | 0.23±0.05 | 1443±100                  | 11.0±10.3           | 169.5±11.7          | −0.5±3.2            |
| WD 0126+101  | 0.19±0.01 | 1680±17                   | 51.3±2.4            | 197.3±2.0           | −9.4±2.6            |
| WD 0129–205  | 0.15±0.02 | 1707±45                   | −39.8±6.3           | 200.5±5.3           | −17.2±3.1           |
| WD 0137–291  | 0.12±0.05 | 1683±105                  | −17.7±12.5          | 197.5±12.4          | 8.9±3.9             |
| WD 0138–236  | 0.12±0.07 | 1870±204                  | 1.4±24.6            | 218.5±23.9          | −17.3±7.6           |
| WD 0140–392  | 0.11±0.01 | 1773±29                   | −30.4±4.1           | 208.5±3.4           | −13.7±2.9           |
| WD 0151+017  | 0.26±0.07 | 1613±183                  | −66.1±18.8          | 189.3±21.4          | −7.8±11.8           |
| WD 0204–233  | 0.38±0.11 | 1178±207                  | −30.7±22.6          | 138.2±24.3          | −49.8±7.4           |
| WD 0205–304  | 0.31±0.03 | 1341±53                   | −45.1±6.0           | 157.3±6.3           | −26.1±3.0           |
| WD 0209+085  | 0.15±0.02 | 1787±48                   | −43.6±5.0           | 209.0±5.7           | −27.7±4.3           |
| WD 0216+143  | 0.23±0.02 | 2242±34                   | 40.2±3.3            | 261.8±3.9           | 10.9±3.1            |
| WD 0252–350  | 0.90±0.06 | 268±161                   | 146.6±18.5          | 32.4±18.8           | −45.1±5.6           |
| WD 0339–035  | 0.25±0.03 | 1592±84                   | −63.5±7.2           | 186.4±9.8           | 18.8±7.7            |
| WD 0408–041  | 0.24±0.12 | 1751±393                  | 37.7±30.8           | 204.7±46.0          | −3.4±38.0           |
| WD 0416–550  | 0.19±0.05 | 1526±98                   | −13.1±14.5          | 179.0±11.5          | 29.2±12.0           |
| WD 0509–007  | 0.23±0.02 | 2326±45                   | −9.4±3.3            | 270.3±5.1           | −14.3±4.7           |
| WD 0911–076  | 0.13±0.03 | 1727±78                   | −31.9±12.5          | 201.5±9.1           | −1.9±12.7           |
| WD 0939–153  | 0.06±0.02 | 1839±43                   | −18.3±8.0           | 215.5±5.0           | 18.0±7.8            |
| WD 0951–155  | 0.25±0.04 | 2124±58                   | −67.4±11.3          | 248.2±6.7           | 19.4±9.6            |
| WD 0956+020  | 0.07±0.03 | 1744±52                   | 8.6±6.7             | 204.3±6.0           | 46.1±5.7            |

**Table 2.** Kinematic parameters of the white dwarfs  
continued from previous page

| star        | $e$       | $J_z$<br>kpc km s $^{-1}$ | $U$<br>km s $^{-1}$ | $V$<br>km s $^{-1}$ | $W$<br>km s $^{-1}$ |
|-------------|-----------|---------------------------|---------------------|---------------------|---------------------|
| WD 1015–216 | 0.08±0.03 | 1928±64                   | 14.1±12.6           | 226.5±7.5           | −16.4±11.2          |
| WD 1020–207 | 0.24±0.01 | 1432±25                   | −16.2±3.9           | 168.2±2.9           | 15.4±3.7            |
| WD 1102–183 | 0.14±0.01 | 1760±25                   | 40.0±3.5            | 207.2±3.0           | 22.5±3.0            |
| WD 1122–324 | 0.12±0.03 | 1909±44                   | −38.1±9.5           | 224.7±5.2           | −17.4±8.7           |
| WD 1124–293 | 0.21±0.01 | 1897±24                   | 63.0±4.2            | 223.5±2.8           | −19.9±3.2           |
| WD 1126–222 | 0.27±0.02 | 1391±40                   | −32.4±7.0           | 163.6±4.8           | −11.6±5.5           |
| WD 1144–246 | 0.09±0.05 | 1795±108                  | −18.5±19.9          | 212.1±12.9          | −24.9±16.7          |
| WD 1150–153 | 0.09±0.02 | 1747±52                   | 17.1±8.2            | 205.9±6.1           | −10.6±5.9           |
| WD 1155–243 | 0.26±0.03 | 1368±52                   | 5.3±7.8             | 161.6±6.1           | −33.7±7.4           |
| WD 1159–098 | 0.06±0.02 | 1761±48                   | −3.3±5.9            | 207.3±5.7           | −13.6±5.4           |
| WD 1201–001 | 0.13±0.04 | 1749±100                  | −33.5±12.9          | 205.7±11.7          | 12.0±7.1            |
| WD 1204–322 | 0.06±0.02 | 1807±31                   | −17.4±4.5           | 213.3±3.7           | −17.9±4.3           |
| WD 1207–157 | 0.09±0.04 | 1767±89                   | −22.4±13.1          | 208.4±10.5          | −18.1±9.8           |
| WD 1244–125 | 0.11±0.02 | 1706±36                   | −23.0±4.9           | 201.1±4.2           | 8.2±3.6             |
| WD 1326–236 | 0.05±0.02 | 1843±46                   | −13.6±5.6           | 218.0±5.5           | −4.9±5.1            |
| WD 1334–678 | 0.41±0.04 | 1163±56                   | −54.6±8.2           | 137.0±6.6           | 20.1±8.0            |
| WD 1342–237 | 0.06±0.01 | 1802±33                   | 15.7±4.0            | 213.0±3.9           | 17.1±3.8            |
| WD 1344+106 | 0.28±0.02 | 1480±26                   | −60.8±2.9           | 174.2±3.0           | −36.1±3.0           |
| WD 1356–233 | 0.19±0.01 | 1855±26                   | −58.5±3.1           | 218.6±3.0           | −20.5±2.6           |
| WD 1401–147 | 0.19±0.02 | 1524±44                   | −18.7±4.2           | 180.0±5.1           | −11.5±4.1           |
| WD 1422+095 | 0.18±0.01 | 1545±22                   | −13.2±1.8           | 182.1±2.5           | −13.9±2.5           |
| WD 1426–276 | 0.50±0.04 | 987±88                    | 73.2±7.9            | 117.9±10.5          | −68.5±11.0          |
| WD 1448+077 | 0.59±0.04 | −1121±144                 | −151.1±5.5          | −132.6±17.1         | −9.6±4.7            |
| WD 1457–086 | 0.08±0.02 | 1793±75                   | 18.9±6.5            | 213.2±8.9           | −13.3±6.9           |
| WD 1515–164 | 0.23±0.04 | 2101±86                   | 57.0±6.5            | 249.6±10.2          | −8.9±8.8            |
| WD 1524–749 | 0.49±0.02 | −1388±119                 | −136.9±15.4         | −167.3±14.5         | −16.1±10.4          |
| WD 1537–152 | 0.12±0.04 | 1752±121                  | −28.2±8.0           | 208.2±14.4          | 23.9±12.5           |
| WD 1555–089 | 0.24±0.02 | 1549±52                   | 55.1±4.1            | 183.4±6.1           | 20.3±5.1            |
| WD 1609+135 | 0.23±0.01 | 1677±23                   | 65.5±3.9            | 197.6±2.7           | 6.2±3.4             |
| WD 1636+057 | 0.26±0.01 | 1395±31                   | 23.1±4.6            | 164.5±3.6           | 9.4±3.1             |
| WD 1834–781 | 0.48±0.03 | 944±49                    | −55.4±7.2           | 111.5±5.9           | −93.2±6.3           |
| WD 1952–206 | 0.37±0.03 | 1161±51                   | 32.9±2.9            | 137.3±6.0           | −64.1±5.1           |
| WD 1959+059 | 0.29±0.02 | 1343±33                   | 29.8±4.2            | 158.8±3.9           | 34.4±3.4            |
| WD 2007–219 | 0.23±0.01 | 1484±22                   | −35.5±2.6           | 175.0±2.6           | 9.4±2.3             |
| WD 2014–575 | 0.12±0.01 | 1763±29                   | 32.4±3.1            | 208.3±3.4           | −27.7±3.3           |
| WD 2139+115 | 0.19±0.02 | 1769±27                   | −54.5±4.9           | 209.5±3.1           | −62.3±4.9           |
| WD 2151–307 | 0.03±0.02 | 1858±48                   | 3.9±5.3             | 219.9±5.7           | −7.2±4.7            |
| WD 2254+126 | 0.15±0.02 | 1706±30                   | −37.6±5.4           | 201.0±3.5           | −9.7±3.8            |
| WD 2306+124 | 0.10±0.01 | 2057±26                   | 9.2±3.3             | 242.0±3.1           | 4.4±3.2             |
| WD 2311–260 | 0.14±0.08 | 1758±248                  | 2.4±29.6            | 210.2±29.7          | −26.9±12.8          |
| WD 2318–226 | 0.20±0.06 | 1531±123                  | 30.4±14.1           | 181.1±14.6          | −15.1±6.5           |
| WD 2322–181 | 0.33±0.04 | 1578±67                   | −92.4±11.7          | 186.5±7.8           | −30.1±5.0           |
| WD 2326+049 | 0.19±0.01 | 1974±14                   | 55.7±2.4            | 232.1±1.6           | −6.0±2.0            |
| WD 2329–332 | 0.13±0.05 | 2080±105                  | −6.8±12.7           | 246.1±12.5          | −11.4±5.0           |
| WD 2333–049 | 0.23±0.03 | 1914±60                   | 70.2±8.5            | 225.1±7.0           | −0.8±4.6            |
| WD 2333–165 | 0.06±0.01 | 1831±31                   | 17.8±3.7            | 215.5±3.7           | −45.8±2.5           |
| WD 2347–192 | 0.18±0.04 | 2026±104                  | 47.9±12.2           | 238.8±12.3          | 2.3±4.7             |
| WD 2348–244 | 0.23±0.02 | 1621±36                   | 62.1±4.2            | 190.9±4.3           | −26.9±3.0           |
| WD 2349–283 | 0.13±0.03 | 1633±64                   | 9.5±6.6             | 192.5±7.5           | −14.2±2.8           |
| WD 2350–248 | 0.08±0.03 | 1974±64                   | 16.4±7.6            | 232.7±7.5           | −2.1±4.6            |
| WD 2351–368 | 0.85±0.07 | 340±154                   | 77.8±8.0            | 40.1±18.1           | 60.5±3.7            |
| WD 2354–151 | 0.15±0.07 | 1705±183                  | 28.3±22.2           | 200.8±21.6          | −6.6±7.6            |

**Table 3.** Classification values for the thick disk candidates

| star         | $c_{\text{UV}}$ | $c_{\text{J}_{\text{Z}}-\text{e}}$ | $c_{\text{orb}}$ | $c$ | classification       |
|--------------|-----------------|------------------------------------|------------------|-----|----------------------|
| HE 0409–5154 | +1              | +1                                 | +1               | +3  | bona fide thick disk |
| HE 1124+0144 | +1              | +1                                 | +1               | +3  | bona fide thick disk |
| WD 0013–241  | +1              | 0                                  | +1               | +2  | bona fide thick disk |
| WD 0204–233  | –1              | +1                                 | +1               | +1  | probable thick disk  |
| WD 0216+143  | +1              | 0                                  | +1               | +2  | bona fide thick disk |
| WD 0509–007  | –1              | 0                                  | +1               | 0   | thin disk            |
| WD 0951–155  | +1              | 0                                  | +1               | +2  | bona fide thick disk |
| WD 1334–678  | +1              | +1                                 | +1               | +3  | bona fide thick disk |
| WD 1426–276  | +1              | +1                                 | +1               | +3  | bona thick disk      |
| WD 1515–164  | +1              | 0                                  | +1               | +2  | bona fide thick disk |
| WD 1834–781  | +1              | +1                                 | +1               | +3  | bona fide thick disk |
| WD 1952–206  | –1              | +1                                 | +1               | +1  | probable thick disk  |
| WD 2322–181  | +1              | –1                                 | +1               | +1  | probable thick disk  |

**Table 4.** Mean value and standard deviation of  $U$ ,  $V$ ,  $W$  for the twelve thick disk white dwarfs from our sample,  $\sigma(U)$ ,  $\sigma(V)$  and  $\sigma(W)$  from Chiba & Beers (2000) are shown for comparison

|  | $\langle U \rangle$<br>km s $^{-1}$ | $\sigma(U)$<br>km s $^{-1}$ | $\langle V \rangle$<br>km s $^{-1}$ | $\sigma(V)$<br>km s $^{-1}$ | $\langle W \rangle$<br>km s $^{-1}$ | $\sigma(W)$<br>km s $^{-1}$ |
|--|-------------------------------------|-----------------------------|-------------------------------------|-----------------------------|-------------------------------------|-----------------------------|
| Thick disk whited dwarfs from our sample   | –5                                  | 69                          | 180                                 | 58                          | –17                                 | 43                          |
| Thick disk stars from Chiba & Beers (2000) | 46                                  |                             | 50                                  |                             | 35                                  |                             |

**Table 5.** Effective temperatures, surface gravities and masses of the thick disk white dwarf candidates,  $M_{\text{W}}$ ,  $M_{\text{B}}$  denote masses derived from Wood (1995) and Blöcker et al. (1997), respectively

| star         | spectra | $T_{\text{eff}}$<br>K | $\log g$<br>cm s $^{-2}$ | $M_{\text{W}}$<br>$M_{\odot}$ | $M_{\text{B}}$<br>$M_{\odot}$ |
|--------------|---------|-----------------------|--------------------------|-------------------------------|-------------------------------|
| HE 1124+0144 | 2       | 15876                 | 7.685                    | 0.455                         | 0.468                         |
| HE 0409–5154 | 1       | 26439                 | 7.750                    | 0.520                         | 0.517                         |
| WD 0013–241  | 2       | 18328                 | 7.855                    | 0.545                         | 0.536                         |
| WD 0204–233  | 1       | 13176                 | 7.750                    | 0.480                         | 0.483                         |
| WD 0216+143  | 1       | 27132                 | 7.790                    | 0.540                         | 0.530                         |
| WD 0951–155  | 2       | 16963                 | 7.765                    | 0.495                         | 0.499                         |
| WD 1334–678  | 1       | 8958                  | 8.110                    | 0.670                         | 0.649                         |
| WD 1426–276  | 2       | 17525                 | 7.665                    | 0.455                         | 0.467                         |
| WD 1515–164  | 1       | 13927                 | 7.810                    | 0.510                         | 0.507                         |
| WD 1834–781  | 2       | 17564                 | 7.760                    | 0.495                         | 0.498                         |
| WD 1952–206  | 2       | 13741                 | 7.780                    | 0.490                         | 0.496                         |
| WD 2322–181  | 2       | 21478                 | 7.880                    | 0.565                         | 0.559                         |

**Table 6.** Effective temperatures, surface gravities and masses of the halo white dwarf candidates,  $M_{\text{W}}$ ,  $M_{\text{B}}$  denote masses derived from Wood (1995) and Blöcker et al. (1997), respectively

| star        | spectra | $T_{\text{eff}}$<br>K | $\log g$<br>cm s $^{-2}$ | $M_{\text{W}}$<br>$M_{\odot}$ | $M_{\text{B}}$<br>$M_{\odot}$ |
|-------------|---------|-----------------------|--------------------------|-------------------------------|-------------------------------|
| WD 0252–350 | 2       | 17055                 | 7.420                    | 0.350                         | 0.386                         |
| WD 2351–368 | 2       | 14567                 | 7.810                    | 0.510                         | 0.509                         |
| WD 1448+077 | 1       | 14459                 | 7.660                    | 0.440                         | 0.455                         |
| WD 1524–749 | 2       | 23414                 | 7.605                    | 0.450                         | 0.471                         |